Biogeosciences, 22, 5877–5896, 2025 https://doi.org/10.5194/bg-22-5877-2025 © Author(s) 2025. This work is distributed under the Creative Commons Attribution 4.0 License.





# Zinc stimulation of phytoplankton in a low-carbon-dioxide, coastal Antarctic environment: evidence for the Zn hypothesis

Riss M. Kell<sup>1,a,i</sup>, Adam V. Subhas<sup>1</sup>, Nicole L. Schanke<sup>2</sup>, Lauren E. Lees<sup>3</sup>, Rebecca J. Chmiel<sup>1</sup>, Deepa Rao<sup>1</sup>, Margaret M. Brisbin<sup>1</sup>, Dawn M. Moran<sup>1</sup>, Matthew R. McIlvin<sup>1</sup>, Francesco Bolinesi<sup>4</sup>, Olga Mangoni<sup>4</sup>, Raffaella Casotti<sup>5</sup>, Cecilia Balestra<sup>6</sup>, Tristan J. Horner<sup>1</sup>, Robert B. Dunbar<sup>7</sup>, Andrew E. Allen<sup>8,9</sup>, Giacomo R. DiTullio<sup>2</sup>, and Mak A. Saito<sup>1</sup>

University of California, San Diego, CA 92037, USA

Correspondence: Mak A. Saito (msaito@whoi.edu)

Received: 4 April 2025 – Discussion started: 14 April 2025

Revised: 19 July 2025 – Accepted: 29 July 2025 – Published: 22 October 2025

Abstract. The ocean acts as a carbon sink, absorbing carbon from the atmosphere and resulting in substantial uptake of anthropogenic CO<sub>2</sub> emissions. As biological processes in the oceans such as net primary production (NPP) contribute significantly to this sink, understanding how they will shift in response to increasing atmospheric CO2 is necessary to project future ocean carbon storage capacity. Macronutrient and micronutrient resource limitation within the oceans regulates NPP, and while some micronutrients such as zinc (Zn) are present at very low concentrations, their ability to limit NPP has remained unclear. Zn is a key micronutrient used by phytoplankton for a multitude of metabolic functions, yet there have been few observations of its influence on natural oceanic phytoplankton populations. In this study, we observed Zn limitation of growth in the natural phytoplankton community of Terra Nova Bay, Antarctica, in addition to primary iron (Fe) limitation. Shipboard incubation experiments amended with Zn and Fe resulted in significantly

higher chlorophyll a content and dissolved inorganic carbon drawdown compared to Fe addition alone. Zn- and Fe-stress-response proteins detected in incubation and environmental biomass provided independent verification of algal co-stress for these micronutrients. We consider total biomass and low surface ocean  $p\mathrm{CO}_2$  as potential drivers of environmental Zn stress. This study establishes that Zn limitation can occur in the modern oceans, opening up new possibility space in our understanding of nutrient regulation of NPP through geologic time and supporting the need to consider the future of oceanic Zn limitation in the face of climate change.

### 1 Introduction

Primary productivity in the oceans is a key component of the global carbon cycle and is largely controlled by the availability of nitrogen (N), phosphorus (P), and iron (Fe). Yet

<sup>&</sup>lt;sup>1</sup>Department of Marine Chemistry and Geochemistry, Woods Hole Oceanographic Institution, Woods Hole, MA 02543, USA

<sup>&</sup>lt;sup>2</sup>Hollings Marine Laboratory, College of Charleston, Charleston, SC 29424, USA

<sup>&</sup>lt;sup>3</sup>Department of Ecology and Evolutionary Biology, University of California at Irvine, Irvine, CA 92697, USA

<sup>&</sup>lt;sup>4</sup>Department of Biology, Università degli Studi di Napoli Federico II, Complesso di Monte Sant'Angelo,

Via Cinthia 21, 80126, Naples, Italy

<sup>&</sup>lt;sup>5</sup>Department of Integrative Marine Ecology, Stazione Zoologica Anton Dohrn, Villa Comunale, 80121, Naples, Italy

<sup>&</sup>lt;sup>6</sup>National Institute of Oceanography and Applied Geophysics, 34010, Sgonico (TS), Italy

<sup>&</sup>lt;sup>7</sup>Doerr School of Sustainability, Stanford University, Stanford, CA 94305, USA

<sup>&</sup>lt;sup>8</sup>Microbial & Environmental Genomics, J. Craig Venter Institute, San Diego, CA 92093, USA

<sup>&</sup>lt;sup>9</sup>Scripps Institution of Oceanography, Integrative Oceanography Division,

<sup>&</sup>lt;sup>a</sup>now at: Gloucester Marine Genomics Institute, Gloucester, MA 01930, USA

ipreviously published under the name Riss Kellogg

there is increasing evidence that other micronutrients such as zinc (Zn), cobalt (Co), and vitamin  $B_{12}$  can also influence phytoplankton productivity, often as secondary limiting nutrients after N, P, or Fe are added (Browning and Moore, 2023; Moore et al., 2013). Zn can be particularly scarce in the photic zone (Bruland, 1980; Jakuba et al., 2012) where total dissolved Zn (dZn<sub>T</sub>) can be below 0.2 nM in seawater due to biological uptake and complexation by organic ligands (Baars and Croot, 2011; Bruland, 1989; Lohan et al., 2002; Middag et al., 2019), which further lowers Zn bioavailability (Lhospice et al., 2017; Saito et al., 2008; Sunda and Huntsman, 2000). Marine eukaryotic algae and copiotrophic bacteria possess a large metabolic demand for Zn that is on par with that of Fe (Mazzotta et al., 2021; Sunda and Huntsman, 2000).

Vertical profiles of dZn in the Southern Ocean have been measured previously. Zn has not historically been considered as a limiting micronutrient in the Southern Ocean due to the upwelling of nutrient-rich waters that bring dZn to nanomolar concentrations only a couple hundred meters below the surface. Yet nutrient-like profiles of dZn are evident throughout this region, with surface depletion due to biological uptake decreasing this large inventory in the upper water column (Baars and Croot, 2011; Coale et al., 2005; Fitzwater et al., 2000; Kell et al., 2024; Sieber et al., 2020). Additionally, both model-based estimates (Roshan et al., 2018) and direct field measurements (Kell et al., 2024) of Zn uptake in this region have demonstrated a substantial biological demand for Zn in surface waters, leading to significant dZn drawdown. This is consistent with genomic and laboratory studies indicating an elevated Zn demand in polar phytoplankton (Twining and Baines, 2013; Ye et al., 2022).

Despite the scarcity of bioavailable Zn in the surface ocean and its high cellular demand, relatively few experimental studies have examined the ability of Zn addition to stimulate natural phytoplankton communities (Table S1 in the Supplement). These results have been variable with findings that include negative results (Coale et al., 2003; Ellwood, 2004; Scharek et al., 1997), slight Zn stimulatory results (Crawford et al., 2003), a "very small increase" relative to controls in an unreplicated experiment (Coale et al., 2003), Zn stimulation within Fe and Si uptake experiments (Franck et al., 2003), Zn primary and secondary limitation in the North Pacific in an unreplicated experiment (Jakuba et al., 2012), secondary Zn limitation after primary Si limitation in the Costa Rica Dome (Dreux Chappell et al., 2016), and enhanced Zn uptake rates under low  $pCO_2$  (Xu et al., 2012). Whether due to the early negative results, the few positive findings, or the practical constraints of co-limitation studies in the field that limit the number of micronutrients that can be tested, there is currently no broad community recognition that zinc limitation is a process that could affect primary productivity in any region of the oceans, leaving the original "zinc hypothesis" unresolved (Morel et al., 1994).

In contrast, laboratory studies have unequivocally demonstrated that marine phytoplankton can easily be Zn-limited in culture and that Zn stress is exacerbated by low CO<sub>2</sub> due to an inability to synthesize the metalloenzyme carbonic anhydrase and resultant carbon co-limitation (Buitenhuis et al., 2003; Morel et al., 1994; Sunda and Huntsman, 2005). In this study, we reconcile these perspectives with a comprehensive, multipronged study of the natural phytoplankton assemblage in Terra Nova Bay (TNB), Antarctica, documenting evidence of Fe and Zn stress in a low-pCO<sub>2</sub> coastal environment.

#### 2 Results

### 2.1 Biogeochemical characterization of Terra Nova Bay

A total of 26 stations within Terra Nova Bay (TNB) were temporally sampled over the course of 1 month (9 January–18 February 2018) during the 2017–2018 CICLOPS expedition (Fig. 1a; Table S2 in the Supplement) to concurrently characterize the natural progression of the phytoplankton bloom and biogeochemical changes in the water column (Kell et al., 2024). These stations were spatially distinct (each unique station was sampled once), but given that all stations were in relatively close proximity to each other within TNB (within a 52 km radius), we have combined all TNB station data to create a temporal analysis of the region.

Surface waters within TNB had low ( $\sim 200 \,\mu atm$ ) seawater pCO<sub>2</sub> (Fig. 1b), which contrasted with measurements  $> 400 \,\mu atm$  further from the study site (Fig. 1c). A large phytoplankton bloom was present as indicated by high  $(> 3000 \,\mathrm{ng}\,\mathrm{L}^{-1})$  chlorophyll fluorescence concentrations in January that waned into February (Fig. 1d). This observation of high productivity is characteristic of Antarctic polynya environments, which are recurring regions of open water surrounded by sea ice (Arrigo et al., 2012). This phytoplankton community initially consisted of a mixed assemblage of both diatoms as indicated by fucoxanthin (fuco, Fig. 1e) and the haptophyte *Phaeocystis* as verified by shipboard microscopy and as indicated by 19'-hexanoyloxyfucoxanthin (19'-hex, Fig. 1f). Surface fucoxanthin concentrations  $> 200 \,\mathrm{ng} \,\mathrm{L}^{-1}$ were observed at the late TNB stations (Fig. 1e), while 19'hex decreased to  $\sim 20 \,\mathrm{ng} \,\mathrm{L}^{-1}$  (Fig. 1f), indicating that the stations sampled in late February were dominated by diatoms rather than Phaeocystis. This was consistent with historical observations of phytoplankton succession patterns in TNB (DiTullio and Smith, 1996; Mangoni et al., 2019; Smith et al., 2006). Additionally, we observed pronounced depletion of total dissolved Zn in surface waters across all TNB stations, with an average concentration of  $0.82 \pm 0.47$  nM at 10 m (Fig. 1g). Notably, as the bloom progressed, this depletion extended progressively deeper into the water column (Fig. 1g), indicative of strong Zn uptake and export from the euphotic zone.

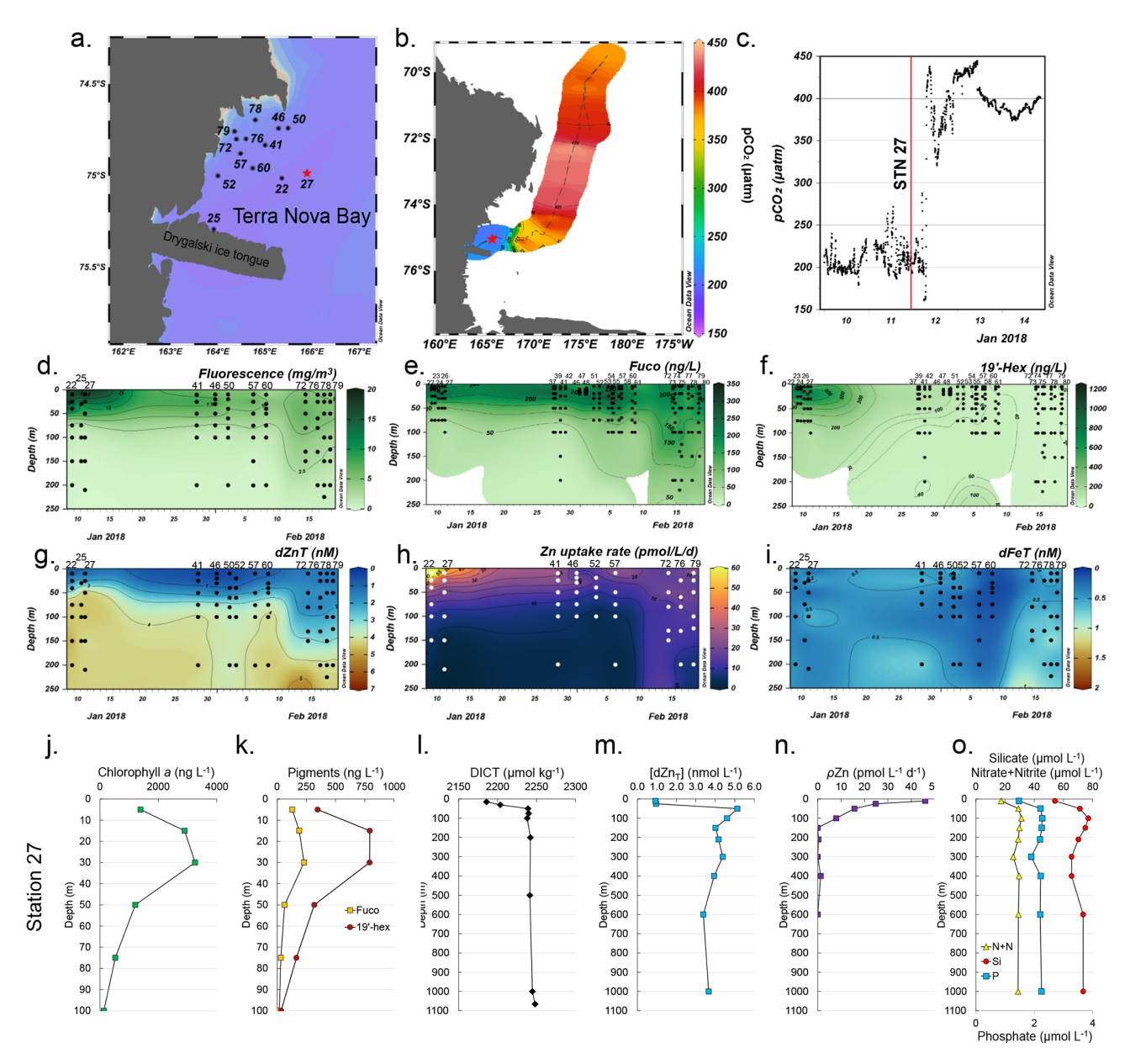


**Figure 1.** Temporal biogeochemistry of Terra Nova Bay and characterization of the experimental site at Station 27. (a) Sampling locations over the Ross Sea shelf in Terra Nova Bay, Antarctica. (b) Location of station 27 (red star) and surrounding seawater  $pCO_2$  measured over a 3 d transit northwards represented in color scale. (c)  $pCO_2$  measured over time within TNB during the 3 d transit shown in (b). The vertical red line denotes the  $pCO_2$  level at the time of initial seawater collection at Station 27. (d) Total chlorophyll fluorescence, (e) fucoxanthin (fuco), (f) 19'hexanoyloxyfucoxanthin (19'-hex), (g) total dissolved Zn, (h) total Zn uptake rates, and (i) total dissolved Fe measured in the upper 250 m represented on a color scale. Station data are presented in order of sampling date, from the earliest (Stn 22, early January) to the latest (Stn 79, late February). The data gap between 13–23 January occurred when the ship was unable to sample due to ice-breaking duties for the McMurdo Station resupply ship. Stations indicated in (a) are those where the trace metal rosette (TMR) was deployed; pigment data were supplemented with additional TNB stations using a CTD (Table S2). Depth profiles of (j) chlorophyll a, (k) the pigments fuco and 19'hex, (l) total dissolved inorganic carbon (DICT), (m) total dissolved Zn, (n) total Zn uptake rates, and (o) the macronutrients nitrate + nitrite (N+N), phosphate (P), and silicate (Si) at the study site. Panels (d) and (g-i) were originally presented in Kell et al. (2024) and are reprised here to introduce the environmental context of the study site.

Total Zn uptake ( $\rho$ Zn, measured concurrently using a stable isotope tracer method) (Kell et al., 2024) was highest in the shallow euphotic zone in early January and waned into February (Fig. 1h), following trends seen in chlorophyll fluorescence (Fig. 1d) and 19'-hex (Fig. 1f). This  $\rho$ Zn trend was consistent with laboratory studies demonstrating the substantial Zn requirements of both diatoms and *Phaeocystis antarctica* (Kellogg et al., 2020; Saito and Goepfert, 2008). Across all TNB stations, total dissolved Fe (dFe<sub>T</sub>) in the upper 50 m remained below 1 nM (Fig. 1i) as observed previously in this region (Fitzwater et al., 2000). In the Ross Sea, dissolved iron (dFe) has previously been demonstrated to be the primary limiting nutrient for phytoplankton growth (Martin et al., 1990; Coale et al., 2003; Sedwick et al., 2011).

# 2.2 Biogeochemical characterization of the incubation study site

Within TNB, Station 27 (referred to as the "experimental site" herein) was chosen for the multifactor shipboard incubation experiment (Fig. 1a and b; red star). This site harbored a coastal bloom, was biologically and chemically characterized as having high in situ chlorophyll a levels (maximum of 3259 ng L<sup>-1</sup> at 30 m; Fig. 1j), and was comprised of diatoms as indicated by fucoxanthin and Phaeocystis as indicated by 19'-hex (Fig. 1k). A decrease in surface total dissolved inorganic carbon (DIC<sub>T</sub>;  $2181 \,\mu\text{mol kg}^{-1}$  at 15 m compared to the deepwater (200-1065 m) average of  $2224 \pm 2.1 \,\mu\text{mol kg}^{-1}$ , Fig. 11) was also observed. Within the water column, dZn demonstrated a pronounced decrease from 5.1 nM at 50 m to 0.9 nM at 10 m, representing an 82 % decrease (and a 76 % decrease comparing the minimum dZn<sub>T</sub> value at 10 m to the average deepwater (210-1000 m) concentration of 3.9 nM  $\pm$  0.4; Fig. 1m), consistent with prior observations of surface dZn depletion in this region (Fitzwater et al., 2000).

Observations of rapid Zn uptake  $(46 \,\mathrm{pmol}\,\mathrm{L}^{-1}\,\mathrm{d}^{-1}$  at  $10 \,\mathrm{m}$ ) at the experimental site (Fig. 1n) likely contributed to this surface depletion, as Zn uptake rates of this magnitude are of the appropriate scale to induce multi-nanomolar surface water depletion during the austral spring and summer season (Kell et al., 2024). Consistent with high macronutrient abundance in this region, surface macronutrient concentrations were partially depleted at the experimental site with  $64 \,\%$ ,  $46 \,\%$ , and  $29 \,\%$  decreases in nitrate + nitrite (N + N), phosphate (P), and silicate (Si), respectively, comparing  $10 \,\mathrm{m}$  and average deepwater  $(200-1000 \,\mathrm{m})$  values (Fig. 1o).

# 2.3 Evidence for Zn stimulation of phytoplankton: experimental site shipboard incubations

A multifactor incubation experiment was conducted using surface waters collected at the experimental site by a tracemetal-clean fish sampler (7 m) fed into a shipboard clean room to examine controls on net primary productivity, with triplicate treatments of Zn-amended (+Zn; 2 nM as ZnCl<sub>2</sub>), Fe-amended (+Fe; 1 nM as FeCl<sub>2</sub>), and Fe- and Zn-amended (+Fe+Zn) incubations, in addition to unamended controls. Addition of Fe alone (+Fe) resulted in significantly higher chl a content compared to controls  $(p = 9.5 \times 10^{-5})$  after 6 d (T6) (Fig. 2a), demonstrating primary Fe limitation as observed previously in the Ross Sea (Mangoni et al., 2019; Martin et al., 1990). However, addition of Zn alone (+Zn) also resulted in significantly higher chl a content compared to the controls (p = 0.011), implying that a subset of the incubated phytoplankton population benefitted from the addition of Zn alone, without additional Fe (Fig. 2a). This observation is consistent with independent co-limitation (Saito et al., 2008), where two nutrients (such as Fe and Zn) each independently limit different subpopulations or processes, and adding either nutrient alone yields a response. The combined addition of +Fe + Zn resulted in the highest average chl a content among all treatments at T6, with  $4.5 \pm 0.21 \,\mu g \, L^{-1}$ compared to  $3.9 \pm 0.35$  and  $2.8 \pm 0.15 \,\mu\text{g}\,\text{L}^{-1}$  achieved by +Fe and +Zn alone, respectively, demonstrating additive colimitation between Zn and Fe (Sperfeld et al., 2016). The Zn stock solution was analyzed to confirm that these results were not caused by inadvertent Fe contamination (see "Materials and methods"). Significant differences in seawater chemistry were also observed within these incubations over time, with larger decreases in DIC<sub>T</sub> in all metal treatments compared to the control  $(-12.7 \,\mu\text{mol kg}^{-1} \text{ for } +\text{Fe}$  $(p = 5.3 \times 10^{-6})$ ,  $-8.2 \,\mu\text{mol kg}^{-1}$  for  $+\text{Zn} \ (p = 5 \times 10^{-5})$ , and  $-18.5 \,\mu\text{mol kg}^{-1}$  for  $+\text{Fe} + \text{Zn} \ (p = 2.2 \times 10^{-16})$ ; Fig. 2b). The decrease in  $DIC_T$  observed with +Fe+Znwas significantly larger than that achieved with +Fe alone  $(p = 4.4 \times 10^{-3}; \text{Fig. 2b})$ . Statistically significant differences in measured parameters among treatments are summarized in Table S3 in the Supplement.

Further consistent with the observed Zn stimulation of biomass in the incubations, the largest decreases in macronutrient (P and N+N) concentrations in these incubations at T6 were observed in the +Fe+Zn treatment (Fig. S1a and b in the Supplement), as was the largest increase in particulate organic carbon (POC; Fig. S1c). POC collected from the +Zn and +Fe+Zn incubations was characterized by larger C: N atomic ratios (5.9 and 6.2, respectively) compared to the +Fe and T6 control (5.2 and 5.3; Fig. S1d). Significantly higher bacterial abundances in both +Fe ( $p=9.1\times10^{-4}$ ) and +Fe+Zn ( $p=6.3\times10^{-4}$ ) treatments relative to the T6 control (Fig. S1e) indicated the alleviation of bacterial Fe limitation, consistent with prior reports (Fourquez et al., 2020; Obernosterer et al., 2015; Sun et al., 2021).

At the conclusion of the incubation experiments, biomass was collected by serial filtration through 5 and  $0.2 \,\mu m$  filters, and the 0.2–5  $\mu m$  fraction was extracted for proteomic analysis (see "Materials and methods") and analyzed for biomarkers of Zn and Fe stress. We detected both algal Fe- and Zn-stress proteins, which provided an independent line of evidence corroborating the results described above (Fig. 2c).

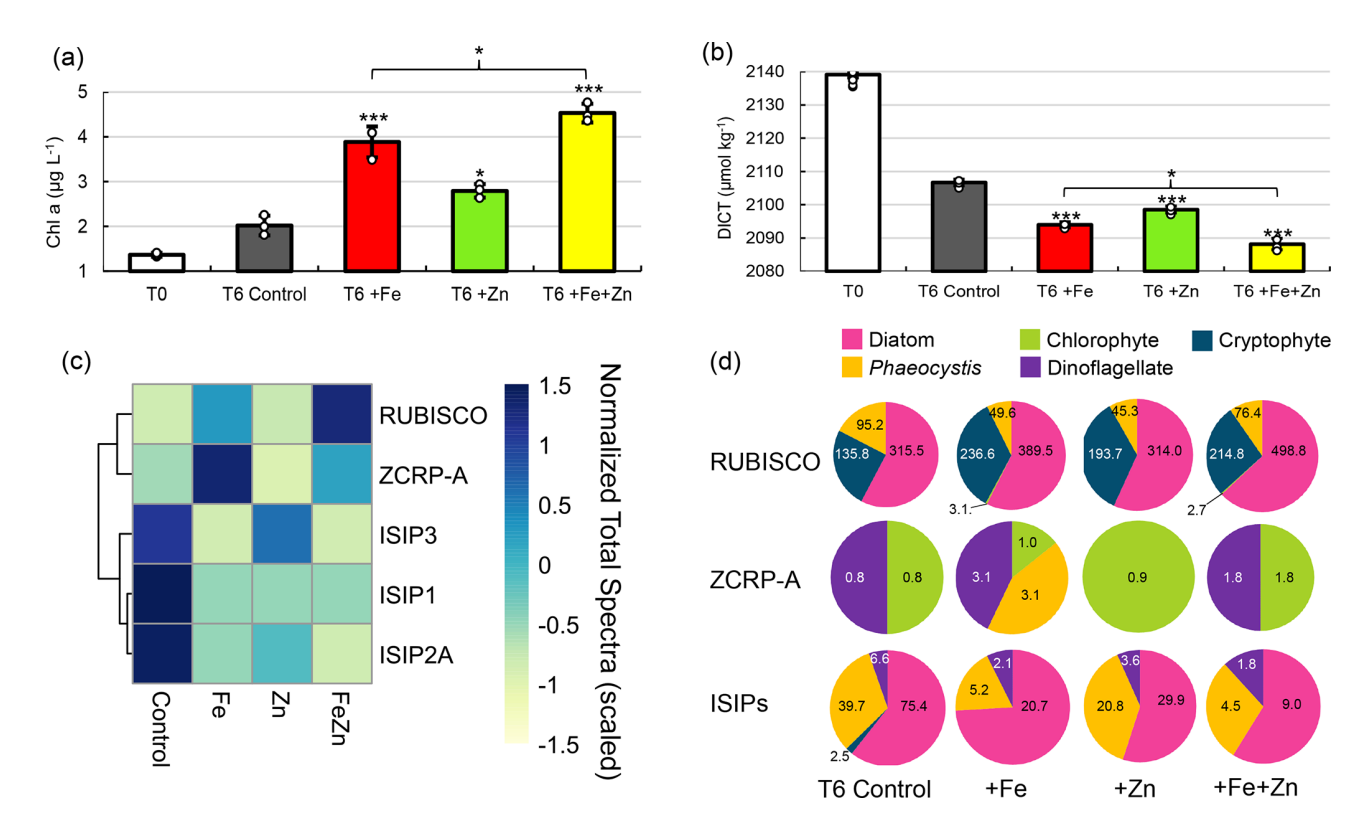


**Figure 2.** Evidence for Zn co-limitation with Fe in bottle incubations. (a) Chlorophyll a and (b) total DIC (DICT) at T0 (day 0) and in each treatment at T6 (day 6). Significant differences among groups were found using one-way ANOVA and a post hoc Dunnett test (\*\*\* p < 0.001, \*\* p < 0.01, \* p < 0.05). Error bars are the standard deviation of biological triplicates (n = 3). Individual data points are overlaid (white circles). (c) Heatmap of row-scaled exclusive protein spectral counts (normalized total spectra) showing relative protein abundance in each treatment. The dendrogram shows similarity in spectral abundance among samples based on Euclidean distance and hierarchical clustering. Color gradients represent low (yellow) to high (blue) protein expression. Ribulose-1,5-biphosphate carboxylase/oxygenase (RUBISCO), zinc/cobalt-responsive protein A (ZCRP-A), and iron-starvation-induced proteins (ISIP1, ISIP2A, ISIP3) are shown. (d) Taxonomies assigned to RUBISCO, ZCRP-A, and ISIP proteins in each treatment at T6. Counts (normalized total spectra) assigned to each taxa are shown. ISIPs are the combined spectral counts of ISIP1A, ISIP2A, and ISIP3.

This included the detection of the Zn/Co-responsive protein ZCRP-A (a putative Zn chaperone) (Kellogg et al., 2022a) as a biomarker of Zn stress as well as the iron-starvationinduced proteins ISIP1A, ISIP2A, and ISIP3 (ISIPs) as biomarkers of Fe stress (Table S4 in the Supplement). The ISIPs represent a group of unrelated proteins that are upregulated under Fe limitation in various algal species. ISIP1 proteins are responsible for endocytosis of siderophore-bound iron, ISIP2 proteins are involved in Fe<sup>3+</sup> uptake, and ISIP3 has been suggested to act as an Fe storage protein (Allen et al., 2008; Behnke and LaRoche, 2020). RUBISCO abundance within each treatment is shown in Fig. 2c as a proxy for the potential phytoplankton production. Within the T6 incubation biomass, there was an increased abundance of ISIPs in the control and +Zn treatment and a decrease in ISIP protein abundance within the +Fe and +Fe + Zn treatments, consistent with primary Fe limitation and the expected response to Fe addition (Fig. 2c). ISIPs were taxonomically assigned to diatoms, *Phaeocystis*, and dinoflagellates (Fig. 2d). The strongest expression of ZCRP-A protein was detected

in the +Fe treatment (Fig. 2c and d), indicative of Fe addition driving the community towards increased Zn stress. Notably, ZCRP-A was still detected in the +Fe + Zn treatment (Fig. 2c and d), implying that the added Zn was unable to completely satiate Zn demand as phytoplankton biomass increased (as indicated by the increase in chl a at T6, Fig. 2a), despite added Zn (2nM) being double that of added Fe (1 nM). Sequence analysis of the contigs identified as ZCRP-A homologs in these incubations revealed that all contigs contained one or more canonical conserved motifs found in COG0523 family proteins such as ZCRP-A (Fig. S2 in the Supplement). Coupled with evidence from prior laboratory studies (Kellogg et al., 2022a), this provides further support for the role of ZCRP-A in responding to Zn scarcity. ZCRP-A proteins were taxonomically assigned to chlorophytes, dinoflagellates, and Phaeocystis, with the detection of Phaeocystis ZCRP-A only in the +Fe treatment (Fig. 2d). The detection of ZCRP-A was attributed to Phaeocystis, but the nondetection of ZCRP-A attributed to diatoms implies that either ample diatom biomass was not captured on the analyzed filters due to being filtered out by the 5 µm pre-filter or diatoms present in these incubations (as indicated by diatom RUBISCO; Fig. 2d) were outcompeting *Phaeocystis* for Zn. Our observations of Fe and Zn biomarkers shifting in abundance in response to their respective metal treatment provides independent evidence for Zn/Fe co-limitation.

#### 2.4 Taxonomic characterization of incubation results

To characterize the phytoplankton species responding to metal amendment, we measured phytoplankton pigments within the shipboard incubations over time, which revealed a diverse taxonomic response to metal amendments. Measured pigments included fucoxanthin (fuco), 19'-hexanoyloxyfucoxanthin (19'-hex),prasinoxanthin (prasino), chlorophyll b (chl b), and chlorophyll c3 (chl c3). Fuco is produced by both diatoms and by *Phaeocystis* under certain conditions, while 19'-hex and chl c3 are indicative of Phaeocystis in the Southern Ocean (DiTullio et al., 2007). Fuco: 19'-hex ratios significantly increased in the +Fe  $(p = 4.2 \times 10^{-4})$  and +Fe + Zn treatments  $(p = 2.7 \times 10^{-3})$ (Fig. S3a in the Supplement) due to no significant change in fuco (Fig. S3b) and decreased 19'-hex (Fig. S3c) relative to the T6 control. Phaeocystis contributions to total fuco concentrations are typically minimal at the low Fe levels of the Ross Sea, though Phaeocystis can revert to making fuco rather than 19'-hex when released from Fe limitation (DiTullio et al., 2007), as was evident in these incubations by decreased 19'-hex: chl c3 ratios within the +Fe and +Fe+Zn treatments (Fig. S3d). Phaeocystis therefore likely contributed to total fuco by responding to Fe addition. Notably, significant decreases in both fuco: chl a and 19'-hex: chl a (Fig. S3e and f) in all treatments compared to the T6 control indicated that other phytoplankton groups contributed to chl a (Fig. 2a) without contributing fuco or 19'hex. Increases in chl b (Fig. S3g) and prasinoxanthin (Fig. S3h) suggest that small green algae such as chlorophytes and prasinophytes also responded to +Fe and +Zn independently, consistent with the detection of chlorophyte ZCRP-A in these incubations (Fig. 2d). Photosynthetic efficiency of photosystem II (Fv/Fm) significantly increased with +Fe (p = 0.011) and with +Fe + Zn (p = 0.0036) at T4 (day 4) compared to T4 controls but did not significantly increase with +Zn alone, implying that Fv/Fm may not be useful as a diagnostic for Zn stress and that caution should be used in interpreting its signals universally (Fig. S3i). No significant difference in Fv/Fm was observed among treatments at T6. Selective zooplankton grazing on small diatoms and solitary *Phaeocystis* cells may have played a role in affecting phytoplankton biomass and the observed pigment: chl a ratios. For instance, higher ratios of phaeophytin: total phaeopigments were observed in +Fe and +Zn amended incubations (Fig. S4 in the Supplement), which may reflect grazing on solitary Phaeocystis cells, as high phaeophytin: total phaeopigment ratios were previously observed in *Phaeocystis*-dominated waters of the Ross Sea (DiTullio and Smith, 1996).

## 2.5 Detection of Zn- and Fe-stress protein biomarkers in the water column

Metaproteomic and metatranscriptomic analyses of biomass within the water column at the experimental site provided additional confirmation of the incubation results, as we detected Zn- and Fe-stress-response proteins present within the water column, which were therefore naturally present without influence from incubation conditions. In addition to ISIPs and ZCRP-A, we detected ZCRP-B (a putative membranetethered Zn-binding protein) (Kellogg et al., 2022a), Zrt/Irtlike (ZIP) transporters (which are known to be used by marine phytoplankton for uptake of Zn<sup>2+</sup> and other divalent metal cations; Allen et al., 2008; Bender et al., 2018; Milner et al., 2013), and  $\theta$  (theta) and  $\delta$  (delta) carbonic anhydrases (CAs).  $\theta$ -CAs with Zn<sup>2+</sup> coordination sites have been documented in diatoms (Jensen et al., 2020a), including the polar diatom Chaetoceros neogracile RS19 (Kellogg et al., 2022b), but no studies to date have investigated enzyme activity or efficiency with  $Co^{2+}$  or  $Cd^{2+}$ . In contrast,  $\delta$ -CA (i.e., *Thalas*siosira weissflogii TWCA1) is known to function with either Co<sup>2+</sup> or Zn<sup>2+</sup> as a cofactor (Lane and Morel, 2000b) conferring metabolic flexibility when Zn<sup>2+</sup> is scarce.

Both proteins and transcripts of Zn and Fe stress biomarkers (ZCRP-A and ISIPs) were observed throughout the water column at the experimental site. RUBISCO, ZCRP-A, and ISIP protein spectral counts were most abundant at the surface and decreased with depth within the 3 µm size fraction (Fig. 3a-c), consistent with the depletion of trace metals in the photic zone due to high-biomass-bloom conditions. ZCRP-A was detected in both 3 and 51 µm filter pore size fractions (Fig. 3b) and was predominantly attributed to Phaeocystis and the diatom genus Chaetoceros in the euphotic zone and predominantly to *Phaeocystis* and the diatom genus Pseudo-nitzschia in the mesopelagic zone (Fig. 3i, Fig. S5a in the Supplement). The presence of *Phaeocystis* below the photic zone is consistent with prior observations of rapid export of *Phaeocystis* cells (DiTullio et al., 2000). Throughout the water column, ISIPs were predominantly attributed to Phaeocystis and to the diatom genera Fragilariopsis, Chaetoceros, and Pseudo-nitzschia (Fig. 3i, Fig. S5b). We note that ZCRP-B, a protein also found to be upregulated in marine diatoms under low Zn/Co and characterized as a putative membrane-tethered Zn/Co protein ligand (Kellogg et al., 2022a), was most abundant in the 0.2 µm fraction throughout the water column (Fig. 3d). As ZCRP-B shares  $\sim 30\%$  similarity to the bacterial ABC-type nickel transporter component NikA, spectral counts within the bacterial 0.2 µm fraction most likely reflect true bacterial NikA. BLAST analysis of all ZCRP-B contigs confirmed that all ZCRP-B hits across all size fractions corresponded to bacteria (Fig. 3i).

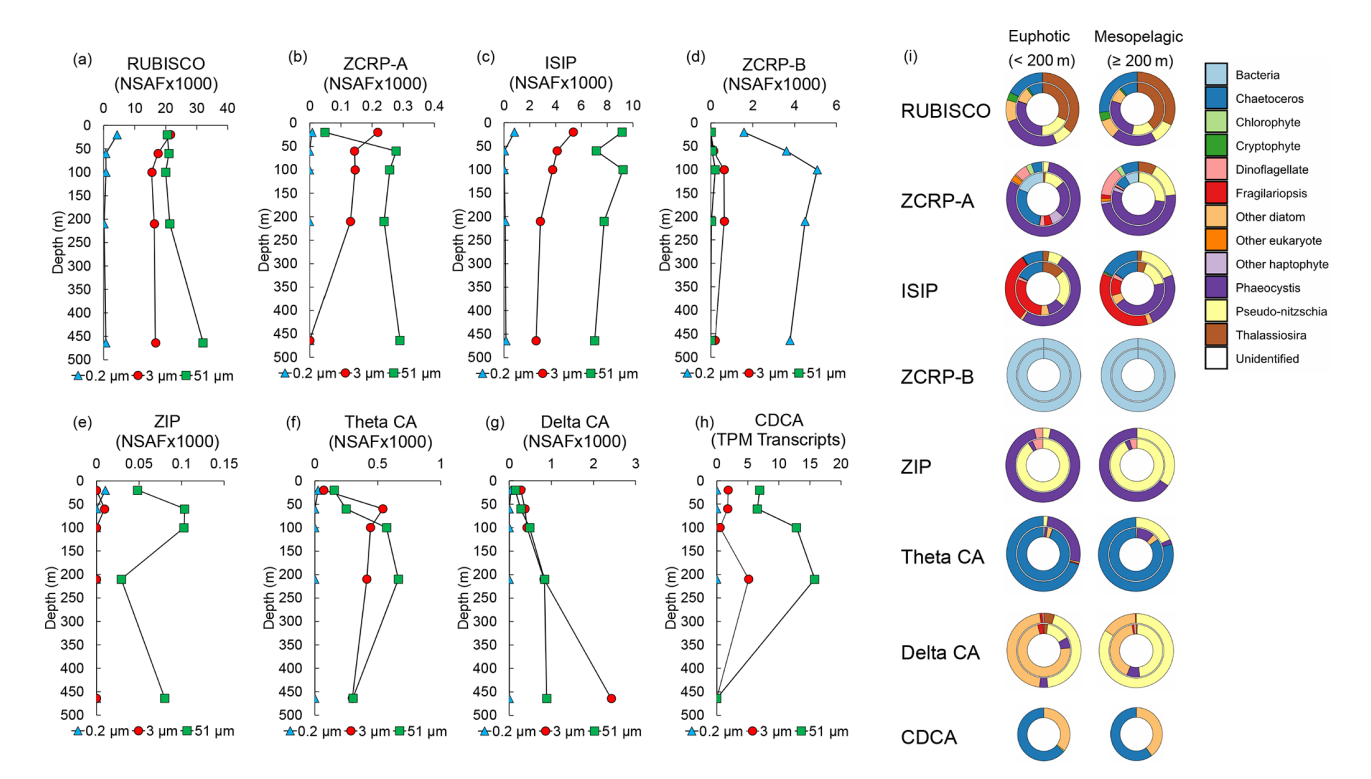


Figure 3. Metatranscriptomic and metaproteomic detection of Zn- and Fe-related proteins of interest at the experimental site. Depth profiles of summed NSAF-normalized protein spectral counts of (a) RUBISCO, (b) ZCRP-A, (c) iron-starvation-induced proteins (ISIPs), (d) ZCRP-B, (e) ZIP, (f) theta CA, and (g) delta CA detected from proteomic analysis of each filter size fraction (0.2, 3, and 51  $\mu$ m). (h) TPM-normalized transcript read counts of CDCA. (i) Stacked pie charts depicting relative community composition for proteins of interest for euphotic (< 200 m) and mesopelagic ( $\geq$  200 m) depths. The outer rings show community composition based on NSAF-normalized protein spectral counts, while the inner rings are TPM-normalized transcript read counts. Protein and transcript counts plotted in (i) were summed across all size fractions. ISIPs are the combined spectral counts of ISIP1A, ISIP2A, and ISIP3.

The assignment of the majority of ZCRP-A and ISIP proteins to Phaeocystis in the upper water column provides additional evidence that *Phaeocystis* was likely Zn/Fe co-limited at the study site, consistent with incubation results (Fig. 2d). ZCRP-A belongs to the phylogenetically complex COG0523 family, with some family members showing functional divergence (that is, activity using different metal cofactors) among paralogs (Blaby-Haas and Merchant, 2012; Edmonds et al., 2021). Here, we infer a Zn-responsive function for the identified ZCRP-A contigs based on their homology to T. pseudonana and P. tricornutum ZCRP-A proteins, which we have previously characterized as Zn-responsive (Kellogg et al., 2022a). To further support this inference, we used SHOOT (Emms and Kelly, 2022) to place each ZCRP-A contig within a phylogenetic context. Of the 21 unique contigs assigned as ZCRP-A homologs, 19 were confirmed to be T. pseudonana orthologs, while 2 were assigned as orthologs to the Zn-related COG0523 E. coli proteins YjiA and YeiR, implying a minor prokaryotic source (Table S5). The placement of the majority of these contigs within diatom clades supports our interpretation that these homologs are Zn-related.

ZIP proteins were almost solely detected in the 51 µm fraction, likely due to the capture of abundant *Phaeocystis* colonies and chain-forming diatoms (Fig. 3e; Fig. S5c). ZIP family transporters are functionally diverse and capable of transporting multiple divalent metal cations, including both Zn<sup>2+</sup> and Fe<sup>2+</sup> (Blaby-Haas and Merchant, 2012), with diatom homologs of ZIP1 known to be upregulated under Fe stress (Lampe et al., 2018). Given the co-limitation of Fe and Zn at the study site, it is difficult to determine which metal these ZIP transporters were primarily mediating.

The increased abundance of diatom  $\theta$ -CA and  $\delta$ -CA proteins within the water column (Fig. 3f and g), as well as transcripts for the diatom Cd carbonic anhydrase CDCA, which can replace Zn<sup>2+</sup> with Cd<sup>2+</sup> as the catalytic cofactor (Lane and Morel, 2000a), in the 3 and 51 µm fractions at 200 m (Fig. 3h) was indicative of a sinking, prior diatom bloom event (Subhas et al., 2019).  $\theta$ -CA and  $\delta$ -CA were predominantly taxonomically assigned to the diatom genera *Chaetoceros* and *Pseudo-nitzschia*, respectively, while CDCA transcripts belonged to the diatom genera *Chaetoceros* and *Corethron* (Fig. 3i). The presence of  $\theta$ -CA, but lack of  $\delta$ -CA, assigned to *Chaetoceros* is consistent with pro-

teomic analysis of the polar diatom *Chaetoceros neogracile* RS19 grown in culture under Zn-limiting conditions (Kellogg et al., 2022b).

# 2.6 Zn: P ratios of the surface seawater at the experimental site

A third independent line of evidence for the nutritional influence of Zn scarcity on TNB phytoplankton was obtained from in situ cellular stoichiometry. Particulate Zn: P ratios (Zn:P) analyzed from biomass collected at the surface of this experimental station were consistent with ratios from Zn-limited culture studies. Particulate Zn: C ratios reported previously in Zn-limiting culture studies of the diatom Thalassiosira pseudonana (Sunda and Huntsman, 2005) were converted to Zn: P ratios using the Redfield ratio (Redfield, 1958) (Table S6 in the Supplement). We then compared these ratios and associated growth rates with particulate Zn:P measured within biomass collected at 10, 25, 50, and 100 m at the experimental site. At each of these surface depths, Zn: P measured at the experimental site was  $\sim 2 \times 10^{-4}$  mol : mol, which, in comparison to cultured diatom Zn: P ratios, fell within the range of severely Zn-limited growth rates (Fig. S6 in the Supplement), again demonstrating the propensity for Zn-limited growth in this region and corroborating the incubation results.

#### 3 Discussion

Antarctic waters are not generally considered to be prone to Zn limitation, given that high (> 1 nM) dZn concentrations are typically observed in surface Southern Ocean waters (Coale et al., 2003). However, we observed multiple independent lines of evidence from both the field incubation experiment (chlorophyll, DIC, Zn, and Fe biomarker proteins) and contextual environmental biogeochemical data of the water column at the incubation site (dZn, Zn uptake rates, pigments, cellular Zn: P stoichiometry, metaproteomic, and metatranscriptomic analyses) demonstrating that phytoplankton within Terra Nova Bay of the Ross Sea, Antarctica, were experiencing Zn and Fe nutritional stress.

Multiple factors could be considered as potential drivers in the creation of Zn-limiting conditions in the field, including Zn demand imposed by total biomass and the species comprising this biomass. The phytoplankton bloom observed during this expedition was comprised primarily of diatoms and *Phaeocystis*, consistent with previous Ross Sea seasonal blooms (Arrigo et al., 2012; Mangoni et al., 2019; Smith et al., 2006), which contributed to the observed high Zn uptake rates and thus surface Zn depletion (Kell et al., 2024), resulting in nutrient-like dZn profiles throughout TNB.

Our field observation of Zn limitation was made in an environment characterized by diminished  $pCO_2$ , which we consider as a factor potentially driving Zn stress. We ob-

served a substantial drawdown of surface seawater  $p\text{CO}_2$  to 221 µatm at the incubation site (a  $\sim$  45 % decrease compared to offshore waters in the Ross Sea measured during the same time frame; Fig. 1b). Biology was the driver of this decrease in  $p\text{CO}_2$ , rather than freshwater input from glacial and sea ice melt. This is evident in the physicochemical data, where over the measured salinity range (S = 33.6-34.8), the effect of simple dilution by freshwater input (DIC = total alkalinity = 0) would result in a reduction of  $p\text{CO}_2$  by only  $\sim$  8–9 ppm. The signals we observe are much larger than that, consistent with a large phytoplankton uptake driver. The total alkalinity (TA) also does not change proportionally with DIC in this region, which is also not consistent with dilution driving a conservative mixing of TA and DIC.

Laboratory studies have unequivocally demonstrated that marine phytoplankton can easily be Zn-limited in culture due to their large Zn requirement and that this effect is exacerbated at low pCO<sub>2</sub> (Morel et al., 1994; Sunda and Huntsman, 2005) due to the use of Zn as a required catalytic cofactor within carbonic anhydrase (CA) metalloenzymes (Sunda and Huntsman, 2005). CAs catalyze the reversible dehydration of HCO<sub>3</sub><sup>-</sup> to CO<sub>2</sub>, the substrate required by the carbonfixing enzyme RUBISCO. As HCO<sub>3</sub> constitutes about 90 % of the dissolved inorganic carbon (DIC) pool in the surface ocean, sufficient CA activity prevents carbon stress in marine phytoplankton by ensuring adequate CO<sub>2</sub> supply to RU-BISCO. It has therefore been hypothesized that the combination of high biomass and resulting low CO<sub>2</sub> may cause severe Zn depletion that may limit algal growth rates due to lack of Zn and thus reduced CA activity, thus reducing the availability of carbon for photosynthesis (Morel et al., 1994; Sunda and Huntsman, 2005). This Zn-C limitation relationship is referred to as "biochemically dependent co-limitation", in which the availability of one nutrient is essential for the acquisition or utilization of another nutrient, especially at low concentrations (Saito et al., 2008).

To explore this in the context of our field observations, using the available quantitative constraints on Zn and CO<sub>2</sub> colimitation thresholds available from the literature (see "Materials and methods"), we estimated that the threshold for Zn-CO<sub>2</sub> limitation in culture synthesized across many algae occurs at 259  $\mu$ atm  $pCO_2$ . We then compared this laboratorydetermined Zn/C limitation threshold estimate to both the in situ 221  $\mu$ atm  $pCO_2$  measured at our field study site and the historical, global trend in surface ocean pCO<sub>2</sub> (Fig. 4a and b). Global surface ocean  $pCO_2$  levels are rapidly rising above both the laboratory-estimated 259  $\mu$ atm  $pCO_2$ Zn/C limitation threshold and our field observation value of 221 µatm (Jiang et al., 2023) (Fig. 4a and b). Though only a fraction of the modern-day surface ocean is currently at  $\leq 250 \,\mathrm{ppm} \, p\mathrm{CO}_2$  (predominantly comprised of polar regions; Fig. 4c), this represents a large decrease in oceanic extent compared to only 100 years ago (Fig. 4d). Even though this may move the majority of oceanic regions farther from Zn and C limitation thresholds, there continue to be highly

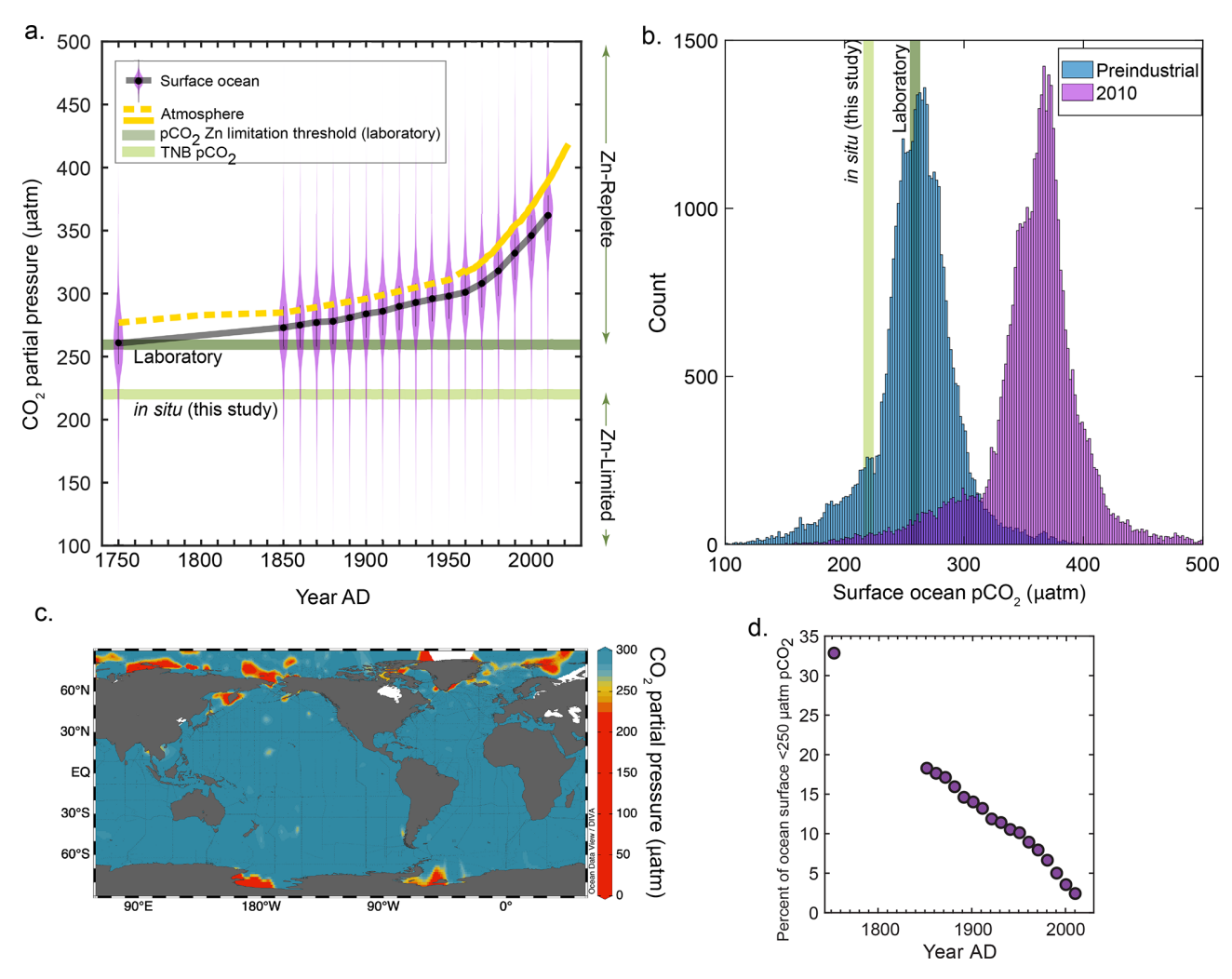


**Figure 4.** The partial pressure of  $CO_2$  ( $pCO_2$ ) and associated phytoplankton responses from this study and the literature. (a) Pre-industrial and decadal surface ocean  $pCO_2$  reconstructions plotted as violin plots, with a running black line through the median values. The atmospheric curve is a composite of ice core data (dashed yellow line; Etheridge et al., 1996) and the Mauna Loa record (solid yellow line; Keeling et al., 1976). An estimated threshold for zinc-limited growth is plotted as the median of previous laboratory results (259  $\mu$ atm, dark green line; see "Materials and methods") and is compared to the in situ results of this study (220  $\mu$ atm, light green line). (b) Data in (a) plotted as a histogram comparing pre-industrial and modern (2010)  $pCO_2$  values, with the same  $pCO_2$  levels indicated. (c) Global map of surface ocean  $pCO_2$  plotted using GLODAPv2.2022 data (Lauvset et al., 2022). (d) Percentage of the ocean surface less than 250  $\mu$ atm  $pCO_2$  as a function of time. Surface ocean  $pCO_2$  reconstructions taken from Jiang et al. (2023).

productive and episodic coastal blooming events that induce significant  $p\text{CO}_2$  drawdown (Dai et al., 2022; Harrison et al., 2018). These coastal regions are increasingly recognized as being disproportionally significant contributors to global ocean carbon export (with respect to their area), particularly at the high latitudes (Dai et al., 2022; Harrison et al., 2018), and will hence continue to be prone to Zn stress at low CO<sub>2</sub> as we have observed. Many other coastal regions have been observed to experience depressed CO<sub>2</sub> such as the Amundsen Sea (Tortell et al., 2012), Amazon River plume (Valerio et al., 2021), the west Florida Shelf (Robbins et al., 2018), the East China Sea (Shim et al., 2007), the northern Gotland Sea (Schneider and Müller, 2018), and Monterey Bay, California

(Chavez et al., 2018), to name a few examples. On the other hand, it is likely that despite rising  $p\text{CO}_2$  levels, some coastal regions will continue to experience episodic or persistent low  $p\text{CO}_2$  due to high productivity (as observed in this study), freshwater inputs, or other regional processes. Though we do not attempt to model future  $p\text{CO}_2$  dynamics in these areas, our results suggest that Zn status may continue to be an important physiological constraint under low  $p\text{CO}_2$  conditions, particularly in productive coastal systems. As such, Zn limitation should be considered as part of the broader framework for understanding carbon cycling in these regions, especially as they play a disproportionate role in global carbon export.

#### 4 Conclusions

The interaction of Zn (and Cd and Co) with CO2 is an important area of future research, particularly in coastal environments. With the continuing rise in atmospheric and surface ocean pCO<sub>2</sub> levels, broader changes in the biogeochemical cycling of Zn and other bioavailable trace metals will likely occur within the oceans, influencing NPP and thus total ocean carbon storage capacity. These low-pCO<sub>2</sub> environments that routinely occur in numerous coastal environments globally should be further examined for Zn effects in addition to carbon uptake dynamics in different temperature environments (Dai et al., 2022; Tortell et al., 2008). While there are elaborate biochemical capabilities available to many marine algae for dealing with Zn scarcity (Kellogg et al., 2022a), our results suggest that the geographic extent of possible Zn/C co-limiting environments may further decrease in the coming decades with rising anthropogenic CO<sub>2</sub> emissions. Despite this, the biochemical demand for Zn in marine organisms remains substantial, with cellular demand rivaling that of Fe. The multitude of metabolic functions requiring Zn, including but not limited to carbonic anhydrase activity, implies the need for further exploration of Zn influences on primary productivity in a changing ocean environment.

#### 5 Materials and methods

### 5.1 Study area and sample collection

Sample collection occurred during the CICLOPS (Cobalamin and Iron Co-limitation of Phytoplankton Species) expedition (NBP18-01) aboard the RVIB Nathaniel B. Palmer from 11 December 2017–3 March 2018 in the Amundsen Sea and Ross Sea of the Southern Ocean (Fig. 1a). Station metadata are provided in Table S2. All stations were assumed to be representative of TNB during this temporal study (as evident in the total dissolved metal, macronutrient, and chlorophyll a datasets). Water samples for dissolved trace metal analyses were collected using trace metal sampling protocols described previously (Cutter and Bruland, 2012). A tracemetal-clean rosette suspended on a Kevlar line and equipped with 12 8 L X-Niskin bottles (Ocean Test Equipment) was used to collect seawater at depths ranging from 10-600 m. Niskin bottles were transported to a positive-pressure tracemetal-clean shipboard van for filtration upon surfacing. Total fluorescence on the vertical profiles was measured using an ECO chlorophyll fluorometer (Wet Labs) equipped on the rosette. The rosette also included instrumentation for measuring conductivity and temperature (Sea-Bird Electronics).

#### 5.2 Preparation of plasticware

Polyethylene and polycarbonate sampling and incubation bottles were rigorously cleaned to remove trace metal contaminants before use. Bottles were rinsed with  $18.2 \Omega$  Milli-

Q water (Millipore), soaked for 72 h in < 1 % Citranox detergent, rotated, soaked for an additional 72 h, and then rinsed five times with Milli-Q water. Bottles were then filled with 10 % HCl (Baker instar-analyzed) by volume and soaked for a minimum of 1 week, rotated, and soaked for another week. Bottles were then rinsed five times with dilute acid (HCl, pH 2) and stored double-bagged in plastic zip bags. All cleaning work was conducted in a Class 100 clean room.

#### 5.3 Underway seawater $pCO_2$ partial pressure

Surface water *p*CO<sub>2</sub> measurements were conducted aboard the RVIB *Nathaniel B. Palmer* using an underway method consisting of an air-water equilibrator and IR CO<sub>2</sub> analyzer developed and operated by the Lamont-Doherty Earth Observatory (LDEO) group (Takahashi et al., 2020). A complete data report and sensor list are available: https://service.rvdata.us/data/cruise/NBP1801/doc/NBP1801DATA.pdf (last access: 14 December 2024) (https://www.rvdata.us/, last access: 14 December 2024).

#### 5.4 TDIC and POC measurements

Total alkalinity (TA) and dissolved inorganic carbon (DIC) were measured on CTD (conductivity-temperature-depth) and incubation samples in near-real time aboard the NBP. Dissolved inorganic carbon (DIC) and total alkalinity (TA) samples were collected following previously established protocols (Dickson et al., 2007). DIC analyses were conducted within  $\sim 4\,\mathrm{h}$  of collection. We acidified 1.25 mL of sample using an automated custom-built injection and bubble stripping system coupled to an infrared gas analyzer (LI-COR LI7000) and integrated the infrared absorption signal versus time for each stripped gas sample to yield a total mass of CO<sub>2</sub>. Each sample was analyzed in triplicate or greater. Since microbubbles regularly formed as samples warmed between sample acquisition and DIC analysis, every integration curve was visually inspected and those curves that exhibited evidence for bubbles were rejected. Certified reference materials (Dickson CRM batch 169) were analyzed between every three to four unknowns. The estimated precision based upon unknowns (> 860 samples run in triplicate) and CRM replicates (n = 738) was  $\pm 2.0 \,\mu\text{mol kg}^{-1}$  ( $\pm 1 \,\text{SD}$ ). Analyses for TA on filtered samples were completed within  $\sim$  12 h of collection by using a potentiometric titrator (Metrohm 855 Robotic Titrosampler) (DeJong et al., 2015). The estimated precision based on replicate analyses of CRMs (n = 195) was  $\pm 2.6 \,\mu \text{mol kg}^{-1} \,(\pm 1 \,\text{SD}).$ 

# 5.5 Analysis of historical atmospheric and surface ocean *p*CO<sub>2</sub> trends

Decadal surface ocean  $pCO_2$  reconstructions (Jiang et al., 2023) were downloaded, binned by decade, and plotted using the "violinplot" in MATLAB. Atmospheric  $pCO_2$  data were assembled from the running Mauna Loa record (Keel-

ing et al., 1976) and from measurements made on Antarctic firn ice (Etheridge et al., 1996).

# 5.6 Calculation of Zn and pCO<sub>2</sub> co-limitation of phytoplankton thresholds

There are few experimental measurements of Zn and  $p\text{CO}_2$  co-limitation, either in the lab or in situ. This study documented Zn limitation of a natural phytoplankton assemblage in the field at a  $p\text{CO}_2$  of  $\sim 220\,\text{ppm}$ . In the literature, several models exist to interpret co-limitation (Buitenhuis et al., 2003; Saito et al., 2008). For this study we chose to use the biochemically dependent co-limitation model for growth rate  $(\mu)$ :

$$\mu = V_{\text{max}} \frac{[\text{CO}_{2(\text{aq})}]}{\varphi K_{\text{S}} + [\text{CO}_{2(\text{aq})}]},\tag{1}$$

where  $V_{\rm max}$  is the maximum growth rate,  $[{\rm CO}_{2({\rm aq})}]$  is the aqueous  ${\rm CO}_2$  concentration of the growth medium in  $\mu {\rm mol} \, {\rm kg}^{-1}$  of seawater,  $K_{\rm s}$  is the half-saturation constant in  $\mu {\rm mol} \, {\rm kg}^{-1}$  of seawater, and  $\varphi$  is a Zn-dependent growth term:

$$\varphi = \frac{[dZn] + K_{s,Zn}}{[dZn]}.$$
 (2)

Here, the dissolved Zn concentration in the growth medium [dZn] is modified by a Zn-dependent saturation constant  $(K_{s,Zn})$ . Few studies have enough experimental data to robustly establish a kinetic relationship between [dZn] and  $[CO_{2(aq)}]$ , so we compiled several estimates for these terms from the literature. Diatom growth rates under pCO<sub>2</sub> limitation were taken from Riebesell et al. (1993) (Riebesell et al., 1993). Reported pH and temperature measurements for each treatment, a total alkalinity of 2300 µmol kg<sup>-1</sup>, and a salinity of 35 were used to calculate aqueous CO2 concentrations using CO2SYSv3.2.1 (Sharp et al., 2023). Reported  $V_{\text{max}}$  and  $K_{\text{s}}$  for D. brightwellii, T. punctigera, and R. alata were 1.46, 1.30, and  $0.93 d^{-1}$  and 1.4, 1.2, and  $2.1\,\mu\text{mol}\,\text{kg}^{-1}$ , respectively. Values for coccolithophore growth  $(K_s = 0.97 \,\mu\text{mol kg}^{-1}, V_{\text{max}} = 4.7 \,\text{d}^{-1})$  were taken from Krumhardt et al. (2017) (Krumhardt et al., 2017). A value for  $K_{s,Zn}$  of 300 pmol L<sup>-1</sup> was taken from Buitenhuis et al. (2003). This value is for the coccolithophore E. huxleyii generated under varying CO2 and Zn conditions, and Zn response growth curves under single CO<sub>2</sub> conditions (ambient) are similar to other diatoms like T. pseudonana (Sunda and Huntsman, 1995). The value of  $300 \,\mathrm{pmol}\,\mathrm{L}^{-1}$  appears high but is tied to the functional form of the biochemically co-limitation equation (Buitenhuis et al., 2003; Saito et al., 2008). Based on the same dataset and different models for co-limitation, Buitenhuis et al. (2003) arrived at  $K_{s,Zn}$  values ranging from 38 to 300 pmol L<sup>-1</sup>. They calculated Zn limitation alone, at  $CO_2$ -replete conditions, of 19 pmol  $L^{-1}$ . Thus, the chosen value of  $K_{s,Zn}$  is not a reflection of high Zn demand but determined by the functionality of biochemical co-limitation by Zn and C.

To calculate  $\varphi$ , a surface ocean Zn concentration of  $50 \,\mathrm{pmol}\,\mathrm{L}^{-1}$  was assumed (Bruland, 1980; Wyatt et al., 2014). While these concentrations reflect total dissolved Zn, the relationship between bioavailable free Zn and dZn, especially in the field, remains unclear. Equation (1) was then used to calculate effective CO2 concentrations (and thus pCO<sub>2</sub> values) at which growth is halved or, in other words,  $\mu = 0.5 V_{\text{max}}$ . We note that this calculation is distinct from the CO<sub>2</sub> half-saturation constant because of the co-limitation by Zn. The median  $pCO_2$  threshold for 50 % growth from the three diatom species was 278 ppm. Including coccolithophores decreases the median to 259 ppm. These values are slightly higher than the in situ evidence for Zn limitation at 220 ppm presented in the present study. Our results cannot be considered an upper bound for Zn-CO<sub>2</sub> limitation but serve as evidence for growth limitation under those specific environmental conditions.

# 5.7 Analyses of total dissolved metals using isotope dilution

The analysis of total dissolved metals for this expedition has been described previously (Kell et al., 2024). Briefly, seawater was collected shipboard by pressure-filtering X-Niskin bottles through an acid-washed 142 mm, 0.2 µm polyethersulfone Supor membrane filter (Pall) within 3 h of rosette recovery using high-purity (99.999%) N<sub>2</sub> gas and stored at 4 °C. All sample collection occurred shipboard within an on-deck trace-metal-clean van. Samples were acidified to pH 1.7 with high-purity HCl (Optima) within 7 months of collection and were stored acidified at room temperature for over 1 year prior to analysis. This extended acidification time was used to counteract any loss of metal due to adsorption to the bottle walls (Jensen et al., 2020b).

Ouantification of total dissolved Fe, Mn, Ni, Cu, Zn, and Cd was performed using isotope dilution. Acidified seawater samples were spiked with a stable isotope spike solution artificially enriched in <sup>57</sup>Fe, <sup>61</sup>Ni, <sup>65</sup>Cu, <sup>67</sup>Zn, and <sup>110</sup>Cd (Oak Ridge National Laboratory). Concentrations and spike ratios were verified by ICP-MS using a multi-element standard curve (SPEX CertiPrep). Preconcentration of spiked seawater samples for total dissolved metal analysis was performed using the automated solid-phase extraction system seaFASTpico (Elemental Scientific) in offline concentration mode with an initial volume of 15 mL and elution volume of 500 µL (Rapp et al., 2017; Wuttig et al., 2019). Following preconcentration, multi-elemental quantitative analysis was performed using an iCAP-Q inductively coupled plasma mass spectrometer (ICP-MS) (Thermo Scientific). Concentrations of Mn, Fe, Ni, Cu, Zn, and Cd were determined using a six-point external standard curve of a multi-element standard (SPEX CertiPrep), diluted to range from 1–10 ppb in 5 % nitric acid. An indium standard (SPEX CertiPrep) was similarly added

to these standard stocks, diluted to range 1–10 ppb. Instrument injection blanks consisted of 5 % nitric acid in Milli-Q. Standard curve  $R^2$  values were  $\geq 0.98$  for all metals monitored. Method accuracy and precision were assessed using the 2009 GEOTRACES coastal surface seawater (GSC) standard (n = 8; Table S7 in the Supplement), which produced values consistent with consensus results (Kell et al., 2024).

#### 5.8 Macronutrient, pigment, and Fv/Fm analyses

Seawater for macronutrient (silicate, phosphate, nitrate, and nitrite) analyses were filtered through 0.2 µm pore size Supor membrane filters and frozen at sea in acid-washed 60 mL high-density polyethylene bottles until analysis. Macronutrient analyses were conducted with an nutrient autoanalyzer (Technicon Autoanalyzer II) by Joe Jennings at Oregon State University. The chemotaxonomic distribution of phytoplankton pigments was determined using HPLC as described previously (DiTullio et al., 2003). Photosynthetic efficiency of photosystem II (Fv/Fm) was measured using a Phyto PAM phytoplankton analyzer (Walz, Effeltrich, Germany) as described previously (Schanke et al., 2021).

#### 5.9 Bacterial abundance

1 mL samples for heterotrophic prokaryote abundance (HPA) analysis were fixed for 10 min with a mix of paraformaldehyde and glutaraldehyde (1% and 0.05% final concentration, respectively), frozen in liquid nitrogen, and stored at -80°C until analysis. After thawing, samples were stained with SYBR Green (Invitrogen Milan, Italy) using  $10^{-3}$  dilution of stock solution for 15 min at room temperature. Cell concentrations were assessed using a FACSVerse flow cytometer (BD BioSciences Inc., Franklin Lakes, USA) equipped with a 488 nm Ar laser and standard set of optical filters. FCS Express software was used for analyzing the data and HP was discriminated from other particles on the basis of scatter and green fluorescence from SYBR Green (Balestra et al., 2011).

### 5.10 ICP-MS analysis and Zn uptake rates using <sup>67</sup>Zn

<sup>67</sup>Zn stable isotope uptake experiments were performed to quantify the movement of dissolved Zn to the particulate phase in units of pmol L<sup>-1</sup> d<sup>-1</sup> (Kell et al., 2024). Briefly, unfiltered seawater was collected using the trace metal rosette over a depth range of 10–600 m into 250 mL trace-metal-clean polycarbonate bottles. Bottles were spiked with <sup>67</sup>Zn such that the total added (spiked) concentration of Zn was 2 nM. Immediately after spiking, incubation bottles were sealed, inverted to mix, and transferred to flow-through ondeck incubators for 24 h. Biomass was collected after 24 h by vacuum-filtering each incubation sample at 34.5 kPa (5 psi) onto an acid-cleaned 3 μm pore size acrylic copolymer Versapore filter (Pall) mounted on an acid-cleaned plastic filtration rig. Sample filters were retrieved from storage at −80 °C, removed from cryovials using plastic acid-washed forceps,

and transferred into trace-metal-clean 15 mL PFA vials with 4 mL of 5 % HNO<sub>3</sub> (Optima) containing a 1 ppb indium (In) internal standard. Filters were digested for  $\sim 3.5 \, \text{h}$  at  $140 \, ^{\circ}\text{C}$ using a HotBlock® heating block (Environmental Express, USA) before they were removed and discarded. After evaporating the remaining solution to just dryness, the residue was resuspended in 2 mL of 5 % HNO<sub>3</sub> (Optima) by light vortexing. Process blank filters were digested and processed as sample filters were. This experiment was also carried out using 110Cd as a tracer of Cd uptake in separate incubation bottles (data not shown here). Digests were analyzed in duplicate by ICP-MS using a Thermo ICAP-Q plasma mass spectrometer calibrated to a multi-element standard curve (Spex Certiprep) over a range of 1–20 ppb. Natural Cd and Zn isotope abundances of the standards were assumed to calculate concentrations of <sup>110</sup>Cd, <sup>111</sup>Cd, <sup>114</sup>Cd, <sup>67</sup>Zn, <sup>66</sup>Zn, and  $^{68}$ Zn. Total Zn uptake (pmol $L^{-1}d^{-1}$ ) was calculated using particulate <sup>67</sup>Zn and total water column dZn measurements as described previously (Cox et al., 2014). The particulate metal measurements captured contributions from the active transport of metal into cells, nonspecific metal adsorption to cell surfaces, metal adsorption to non-living particulate organic matter, and metal adsorption to particulate inorganic matter, though we expect active transport into cells to dominate the measured particulate isotopic signal due to the high abundance of actively growing autotrophic cells in the photic zone observed in the Southern Ocean during austral summer. Particulate Zn: P measurements were calculated using particulate Zn measured on Cd-spiked filters and thus do not include any pZn contribution from Zn tracer addition. Particulate phosphorus concentrations were measured by ICP-MS simultaneously and were calibrated to a standard curve ranging from 100 to 3200 ppb using a 1 ppm certified P stock (Alfa Aesar Specpure). All SPEX and P standard curves had  $R^2$  values > 0.99. The Zn stock solution used in the incubation experiments was similarly analyzed by ICP-MS to confirm that the stock was not Fe-contaminated – this analysis showed that less than 2.3 pM (which was near the instrument blank level for this analysis) of iron was added for every 2 nM of zinc, far less than needed to stimulate phytoplankton to the extent observed in our experiments.

### 5.11 Shipboard incubation experiments

Incubation experiments were conducted at Station 27  $(-74.9870^{\circ} \text{ N}, 165.8898^{\circ} \text{ E})$ . Raw surface seawater was pumped directly into a clean-room container van, collected into acid-cleaned 50 L carboys, and dispensed into acid-washed 1 L polycarbonate bottles using a trace metal sampling system with acid-washed polypropylene tubing and a Teflon diaphragm pump. Incubation bottles were first rinsed with seawater, then filled. Seawater was collected at 16:05 UTC. Triplicate incubation bottles were amended with  $+\text{Fe}\,(1\,\text{nM}), +\text{Zn}\,(2\,\text{nM}),$  and  $+\text{Fe}\,+\text{Zn},$  sealed, and placed into a flow-through on-deck incubator with light screens that

shaded the incubator to 20% ambient surface irradiance. Incubations were sampled at 0, 48, 96, and 144 h (corresponding to T0, T2, T4, and T6 time points) for analysis by filtering onto GFF filters for chlorophyll (all time points, biological triplicates), pigment analyses (T6, biological triplicates), and proteomic analyses (T6, pooled biological triplicates). Chlorophyll was extracted immediately; otherwise, samples were frozen at  $-80\,^{\circ}\text{C}$  until further analyses, with pigment and protein samples kept in  $-80\,^{\circ}\text{C}$  freezers, liquid nitrogen dewars, or dry ice coolers at all times during transport back to the laboratories. All amendments and sampling were conducted in a positive-pressure clean-room van with laminar flow hoods and plastic sheeting to minimize trace metal contamination.

#### 5.12 Metaproteomic analysis

Water column metaproteomic biomass was collected onto 0.2, 3, and 51 µm pore size filters ("field filters") using in situ battery-operated McLane pumps. Half of each field filter was processed for metaproteomic analysis. Incubation metaproteomic biomass was serially filtered through a 5 µm pore pre-filter followed by a 142 mm GFF filter. Three-fourths of each GFF filter was used for subsequent metaproteomic analysis of the incubations. All filters were frozen at -80 °C and stored until laboratory extraction. To extract proteins, filters were placed into extraction buffer (1 % SDS, 0.1 M Tris/HCL pH 7.5, 10 mM EDTA). 8 mL of buffer was used for each field filter, and 15 mL of buffer was used for each GFF incubation filter. All reagents were made with HPLCgrade water. Samples were heated at 95 °C for 10 min and shaken at room temperature for 30 min. Filters were removed and protein extracts were filtered through 5.0 µm Millex low-protein-binding filters (Merck Millipore #SLSV025LS). Millex filters were rinsed with 1 mL of extraction buffer to ensure no loss of protein. Samples were then spun for 30 min at 3220 rcf in an Eppendorf 5810 centrifuge. The supernatant was transferred to Vivaspin 5K MWCO ultrafiltration columns (Sartorius #VS0611). Protein extracts were concentrated to approximately 300 µL, washed with 1 mL of extraction buffer, and transferred to a 2 mL ethanol-washed microtube (all tubes from this point on are ethanol-washed). Vivaspin columns were rinsed with small volumes of protein extraction buffer to remove all concentrated protein and samples were brought up to 400 µL with extraction buffer. Samples were incubated with 2 µL benzonase nuclease (EMD Millipore 70746-3) for 30 min at 37 °C.

Extracted proteins were purified from SDS detergent, reduced, alkylated, and digested with trypsin while embedded within a polyacrylamide tube gel, using a modified, previously published method (Lu and Zhu, 2005). A gel premix was made by combining 1 M Tris HCL (pH 7.5) and 40 % Bis-acrylamide L 29:1 (Acros Organics) at a ratio of 1:3. The premix (103  $\mu$ L) was combined with 50–100  $\mu$ g of the extracted protein sample, Tris-EDTA, 7  $\mu$ L 1 % APS,

and 3 µL of TEMED (Acros Organics) to a final volume of 200 µL. After 1 h of polymerization at room temperature, 200 µL of gel fix solution (50 % ETOH, 10 % acetic acid in LC/MS grade water) was added to the top of the gel and incubated at room temperature for 20 min. Liquid was then removed and the tube gel was transferred into a new 1.5 mL microtube containing 1.2 mL of gel fix solution before incubating at room temperature at 350 rpm in a Thermomixer R (Eppendorf) for 1 h. Gel fix solution was removed and replaced with 1.2 mL of destain solution (50 % MeOH, 10% acetic acid in LC/MS grade water) and incubated at 350 rpm and room temperature for 2 h. Liquid was removed, and gels were cut up into 1 mm cubes and added back to tubes containing 1 mL of 50:50 acetonitrile:25 mM ammonium bicarbonate (ambic) and incubated for 1h at 350 rpm and room temperature. Liquid was removed and replaced with fresh 50:50 acetonitrile: ambic solution and incubated at 16 °C and 350 rpm overnight. The above step was repeated for 1 h the following morning. Gel pieces were then dehydrated twice in 800 µL of acetonitrile for 10 min at room temperature and dried for 10 min in a ThermoSavant DNA110 speedvac after removing the solvent. Proteins were reduced in 600 µL of 10 mM DTT, 25 mM ambic at 56 °C and 350 rpm for 1 h. The volume of unabsorbed DTT solution was measured prior to removal. Gel pieces were washed with 25 mM ambic, and 600 µL of 55 mM iodoacetamide was added to alkylate proteins at RT and 350 rpm for 1 h. Gel cubes were then washed with 1 mL ambic for 20 min and 350 rpm at RT. Acetonitrile (1 mL) dehydrations and speedvac drying were repeated as described above. Trypsin (Promega #V5280) was added in an appropriate volume of 25 mM ambic to rehydrate and submerse gel pieces at a concentration of 1:20 µg trypsin: protein. Proteins were digested overnight at 350 rpm at 37 °C. Unabsorbed solution was removed and transferred to a new tube. 50 µL of peptide extraction buffer (50 % acetonitrile, 5 % formic acid in water) was added to gels, incubated for 20 min at RT, then centrifuged at  $14\,100 \times g$  for 2 min. The supernatant was collected and combined with the corresponding unabsorbed solution. The above peptide extraction step was repeated again, combining corresponding supernatants. Combined digested peptides were centrifuged at  $14\,100 \times g$  for  $20\,\text{min}$ , and supernatants were transferred into a new tube and dehydrated down to approximately 20 µL in the speedvac. Total digested peptides were quantified (Bio-Rad DC protein assay, Hercules, CA) with BSA as a standard. Peptides were then diluted in 2% acetonitrile and 0.1% formic acid in LC/MSgrade water to a concentration of  $1 \mu g (\mu L)^{-1}$  for storage until analysis. All water used in the tube gel digestion protocol was LC/MS-grade, and all plastic microtubes were ethanolrinsed and dried prior to use.

Purified peptides were diluted to  $0.1\,\mu g\,\mu L^{-1}$  and  $20\,\mu l$  (2  $\mu g$ ) was injected onto a Dionex UltiMate 3000 RSLC-nano LC system (Thermo Fisher Scientific) with an additional RSLCnano pump run in online two-dimensional ac-

tive modulation mode coupled to a Thermo Fusion Orbitrap mass spectrometer as described previously (McIlvin and Saito, 2021).

A translated metatranscriptome (see below) was used as a reference protein database and peptide spectra matches were performed using the SEQUEST algorithm within Proteome Discoverer v.2.1 (Thermo Fisher Scientific) with a fragment tolerance of 0.6 Da and parent tolerance of 10 ppm. Identification criteria consisted of a peptide threshold of 95 % (false discovery rate (FDR) = 0.1 %) and protein threshold of 99 % (1 peptide minimum, FDR = 0.8 %) in Scaffold v.5 (Proteome Software), resulting in 5387 proteins identified in the incubation experiment and 27 924 proteins identified in the water column. To avoid double-counting mass spectra, exclusive spectral counts were used for the downstream proteomic analysis. Exclusive spectral counts were normalized using the normalized spectral abundance factor (NSAF) calculation (Zhang et al., 2010) to allow for a comparison of protein abundance across samples while remaining consistent with the metatranscriptomic procedure; see Cohen et al. (2021) for details. Counts associated with redundant ORFs (sharing identical taxonomic and functional assignments) were summed together. The stand-alone commandline application BLAST+ from the National Center for Biotechnology Information (NCBI) was used to identify proteins of interest in the metaproteomic data. Metaproteomes were BLAST-searched ( $E = 5 \times 10^{-5}$ ) against the known sequences of proteins of interest acquired from annotated proteomic databases (Table S4) and combined with further annotation data based on contig ID (see below).

### 5.13 Metatranscriptomic analysis

Transcriptomic assemblies were generated for biomass collected using McLane pumps filtered through 0.2, 3, and 51 µm pore size filters. In order to enrich metatranscriptomic libraries derived from 0.2 µm filters in prokaryotic transcripts and libraries derived from 3 and 51 µm filters in eukaryotic transcripts, 0.2 µm libraries were generated from total rRNA-depleted mRNA and 3 and 51 µm libraries were generated from polyA mRNA. Total RNA was extracted from 0.2, 3, and 51 µm filters using a Macherey-Nagel NucleoMag RNA kit (Macherey-Nagel GmbH & Co. KG). Cleared lysate was loaded into a 96-deep-well plate and put on an ep-Motion 5075 TMX liquid handler to complete the RNA extraction following the Machery-Nagel standard protocol. For 3 and 51 µm samples with total RNA greater than 1 µg, 800 ng of total RNA was used for preparing poly A libraries with an Illumina Stranded mRNA Prep Ligation kit (Illumina), following the manufacturer's protocol. For the 3 and 51 µm samples with total RNA less than 1 µg, 20 ng of total RNA was used as input for the SMART-Seq v4 Ultra Low Input RNA kit (Takara Bio USA. Inc), which converts poly(A) RNA to full-length cDNA using a modified oligo (dT) primer with simultaneous cDNA amplification. The resulting double-stranded cDNA was then fragmented using a Covaris E210 system with the target size of 300 bp. Libraries were prepared from fragmented double-stranded cDNA using an Illumina Stranded mRNA Prep Ligation kit (Illumina). For RNA obtained from 0.2 µm filters, ribosomal RNA was removed using a riboPOOL Seawater Kit (Galen Laboratory Supplies, North Haven, Connecticut, USA). The riboPOOL Seawater Kit is a customized mixture of removal solutions: Pan-Prokaryote riboPOOL, Pan-Plant riboPOOL, and Pan-Mammal in a ratio of 6:1:1. The rRNA-depleted total RNA was used for cDNA synthesis by the Ovation RNA-Seq System V2 (TECAN, Redwood City, USA). Double-stranded cDNA was then prepared for the libraries using an Illumina Stranded mRNA Prep Ligation kit (Illumina). Ampure XP beads (Beckman Coulter) were used for final library purification. Library quality was analyzed on a 2200 TapeStation System with an Agilent High Sensitivity DNA 1000 Screen-Tape System (Agilent Technologies, Santa Clara, CA, USA). Resulting libraries were subjected to paired-end Illumina sequencing via NovaSeq 6000 S4.

The input paired-end fastq sequences are trimmed of sequencing adapters, primers, and low-quality bases by using either BLASTN (NCBI, v2.2.25) (Altschul et al., 1990) or trimmomatic, v0.36 (Bolger et al., 2014). The trimmed paired and unpaired sequences were then depleted of rRNA sequences with riboPicker v0.4.3 (Schmieder et al., 2012). The command-line program clc\_assembler, v5.2.1 (Qiagen) was used to assemble processed sequences into contigs and ORFs were identified by FragGeneScan, v1.31 (Rho et al., 2010). The trimmed sequences were mapped to the predicted ORFs using the command-line program clc\_mapper, v5.2.1 (Qiagen) to generate mapped raw read counts for each ORF. The raw counts were normalized initially to RPKM values to account for variations in inter-sample sequencing depth and the ORF sequence length (Mortazavi et al., 2008). The RPKM values were subsequently converted to TPM (transcripts per million) units for estimation of the relative RNA abundance among samples (Li and Dewey, 2011). The ORFs were annotated for putative function by several programs in parallel using BLASTP against PhyloDB, hidden Markov models PFAM and TIGRFAM by HMMER, v3.3.2 (Eddy, 2011), KEGG Ortholog HMM by kofamscan, v1.3.0 (Aramaki et al., 2020), and transmembrane HMM by TMHMM (Krogh et al., 2001). Additional annotations were generated by similarity searches using BLASTP to transporter (PhyloDB), organelle (PhyloDB), and KOG (Tatusov et al., 2003) databases. The ORFs are assigned to the best taxonomic species/group as determined by LPI (lineage probability index) analysis (Podell and Gaasterland, 2007). The final list of curated ORFs was generated by removing ORFs with low mapping coverage (< 50 reads total over all samples), no BLAST hits, and no known domains.

### 5.14 Statistical analysis and data visualization

ANOVA and Dunnett tests were performed using MATLAB 2019a. Statistics are summarized in Table S3. Figures were made using matplotlib (version 3.5.0), Ocean Data View (version 5.5.2; Schlitzer, 2025), Excel (2019), and RStudio (version 1.3.1093). Color palettes used in Ocean Data View section plots (https://doi.org/10.5281/zenodo.8409685, Crameri, 2023) are inverse "roma" for trace metal concentrations, "thermal" for Zn and Cd uptake rates, and "algae" for chlorophyll fluorescence (Crameri, 2023).

(NBP18-01; Data availability. CICLOPS https://doi.org/10.5281/zenodo.17287908, Lampe et al., 2025) conductivity-temperature-depth (CTD) hydrography data including pressure, temperature, total dissolved oxygen, conductivity, fluorescence, and beam transmission (https://doi.org/10.1575/1912/bco-dmo.783911.1; DiTullio and Lee, 2020), as well as total dissolved metal, Zn and Cd uptake rate, macronutrient, and pigment datasets are available through the NSF Biological and Chemical Oceanography Data Management Office (BCO-DMO) repository (https://doi.org/10.7284/907753; DiTullio, 2018). A CICLOPS project data overview page can be found at https://doi.org/10.5281/zenodo.17287908 (Lampe et al., 2025). Underway pCO<sub>2</sub> data collected during cruise NBP1801 are available through R2R at https://doi.org/10.7284/139318 (DiTullio, 2017). The mass spectrometry global proteomic data for CICLOPS water column analyses and bottle incubations have been deposited to the ProteomeXchange Consortium through the PRIDE repository under dataset identifiers PXD037056 and PXD069333, respectively (https://www.ebi.ac.uk/pride/archive/projects/PXD069333,

last access: 30 September 2025). The raw metatranscriptome reads have been deposited in the National Center for Biotechnology Information Sequence Read Archive under BioProject accession no. PRJNA890306 (https://www.ncbi.nlm.nih.gov/bioproject/?term=PRJNA890306, last access: 29 September 2025) and RNA-Seq BioSample accession nos. SAMN31286421–SAMN31286522 (https://www.ncbi.nlm.nih.gov/biosample/?term=SAMN31286421, last access: 29 September 2025). The metatranscriptome assembly and annotation for CICLOPS samples can be accessed at https://doi.org/10.5281/zenodo.17307449.

*Supplement.* The supplement related to this article is available online at https://doi.org/10.5194/bg-22-5877-2025-supplement.

Author contributions. All authors contributed to data acquisition and analysis. RMK, NLS, LEL, RJC, DR, DMM, MRM, FB, RBD, GRD, and MAS implemented the shipboard incubation study. RMK, MMB, RJC, DR, TJH, and AVS contributed to the formal analysis. NLS, LEL, FB, OM, RC, and GRD contributed to pigment datasets and interpretations. CB provided bacterial abundance data. RBD contributed DIC and in situ pCO<sub>2</sub> data. AVS contributed analyses and discussion regarding historical pCO<sub>2</sub> data and Zn–C growth limitation estimates. AEA contributed the metatran-

scriptome reference database used for proteomic analyses. RMK and MAS wrote the original draft. RMK, MAS, GRD, AVS, TJH, and RBD contributed to review and editing. All authors approved the final submitted paper.

Competing interests. The contact author has declared that none of the authors has any competing interests.

Disclaimer. Publisher's note: Copernicus Publications remains neutral with regard to jurisdictional claims made in the text, published maps, institutional affiliations, or any other geographical representation in this paper. While Copernicus Publications makes every effort to include appropriate place names, the final responsibility lies with the authors.

Acknowledgements. We thank the captain, crew, marine technicians, and science party of RVIB Nathaniel B. Palmer for their support and contributions to the success of the NBP18-01 cruise. We thank Natalie Cohen for assistance and training with the SeaFAST. We thank Veronique Oldham for assistance with trace metal sampling. We thank Robert Lampe for data curation and proofreading efforts.

Financial support. This work was funded by the National Science Foundation (grant nos. 2125063, 1643684, 1924554) and the Simons Foundation with grants to Mak A. Saito, NSF-PLR 1643845 to Robert B. Dunbar, and NSF-CO (grant no. 2123055) to Mak A. Saito and Adam V. Subhas, as well as the National Institutes of Health (grant no. GM135709-01A1 to Mak A. Saito).

Review statement. This paper was edited by Emilio Marañón and reviewed by two anonymous referees.

#### References

Allen, A. E., LaRoche, J., Maheswari, U., Lommer, M., Schauer, N., Lopez, P. J., Finazzi, G., Fernie, A. R., and Bowler, C.: Wholecell response of the pennate diatom Phaeodactylum tricornutum to iron starvation, P. Natl. Acad. Sci. USA, 105, 10438–10443, https://doi.org/10.1073/pnas.0711370105, 2008.

Altschul, S. F., Gish, W., Miller, W., Myers, E. W., and Lipman, D. J.: Basic local alignment search tool, J. Mol. Biol., 215, 403–410, https://doi.org/10.1016/S0022-2836(05)80360-2, 1990.

Aramaki, T., Blanc-Mathieu, R., Endo, H., Ohkubo, K., Kanehisa, M., Goto, S., and Ogata, H.: KofamKOALA: KEGG Ortholog assignment based on profile HMM and adaptive score threshold, Bioinformatics, 36, 2251–2252, https://doi.org/10.1093/bioinformatics/btz859, 2020.

Arrigo, K. R., Lowry, K. E., and van Dijken, G. L.: Annual changes in sea ice and phytoplankton in polynyas of the Amundsen Sea, Antarctica, Deep-Sea Res. Part II Top. Stud. Oceanogr., 71–76, 5–15, https://doi.org/10.1016/j.dsr2.2012.03.006, 2012.

- Baars, O. and Croot, P. L.: The speciation of dissolved zinc in the Atlantic sector of the Southern Ocean, Deep-Sea Res. Part II Top. Stud. Oceanogr., 58, 2720–2732, https://doi.org/10.1016/j.dsr2.2011.02.003, 2011.
- Balestra, C., Alonso-Sáez, L., Gasol, J. M., and Casotti, R.: Group-specific effects on coastal bacterioplankton of polyunsaturated aldehydes produced by diatoms, Aquat. Microb. Ecol., 63, 123–131, https://doi.org/10.3354/ame01486, 2011.
- Behnke, J. and LaRoche, J.: Iron uptake proteins in algae and the role of Iron Starvation-Induced Proteins (ISIPs), Eur. J. Phycol., 55, 339–360, https://doi.org/10.1080/09670262.2020.1744039, 2020.
- Bender, S. J., Moran, D. M., McIlvin, M. R., Zheng, H., McCrow, J. P., Badger, J., DiTullio, G. R., Allen, A. E., and Saito, M. A.: Colony formation in *Phaeocystis antarctica*: connecting molecular mechanisms with iron biogeochemistry, Biogeosciences, 15, 4923–4942, https://doi.org/10.5194/bg-15-4923-2018, 2018.
- Blaby-Haas, C. E. and Merchant, S. S.: The ins and outs of algal metal transport, Biochim. Biophys. Acta Mol. Cell Res., 1823, 1531–1552, https://doi.org/10.1016/j.bbamcr.2012.04.010, 2012.
- Bolger, A. M., Lohse, M., and Usadel, B.: Trimmomatic: a flexible trimmer for Illumina sequence data, Bioinformatics, 30, 2114– 2120, https://doi.org/10.1093/bioinformatics/btu170, 2014.
- Browning, T. J. and Moore, C. M.: Global analysis of ocean phytoplankton nutrient limitation reveals high prevalence of co-limitation, Nat. Commun., 14, 5014, https://doi.org/10.1038/s41467-023-40774-0, 2023.
- Bruland, K. W.: Oceanographic distributions of cadmium, zinc, nickel, and copper in the North Pacific, Earth Planet. Sci. Lett., 47, 176–198, https://doi.org/10.1016/0012-821X(80)90035-7, 1980
- Bruland, K. W.: Complexation of zinc by natural organic ligands in the central North Pacific, Limnol. Oceanogr., 34, 269–285, https://doi.org/10.4319/lo.1989.34.2.0269, 1989.
- Buitenhuis, E. T., Timmermans, K. R., and de Baar, H. J. W.: Zinc-bicarbonate colimitation of Emiliania huxleyi, Limnol. Oceanogr., 48, 1575–1582, https://doi.org/10.4319/lo.2003.48.4.1575, 2003.
- Chavez, F. P., Sevadjian, J., Wahl, C., Friederich, J., and Friederich, G. E.: Measurements of *p*CO<sub>2</sub> and pH from an autonomous surface vehicle in a coastal upwelling system, Deep-Sea Res. Part II Top. Stud. Oceanogr., 151, 137–146, https://doi.org/10.1016/j.dsr2.2017.01.001, 2018.
- Coale, K. H., Wang, X., Tanner, S. J., and Johnson, K. S.: Phytoplankton growth and biological response to iron and zinc addition in the Ross Sea and Antarctic Circumpolar Current along 170° W, Deep-Sea Res. Part II Top. Stud. Oceanogr., 50, 635–653, https://doi.org/10.1016/S0967-0645(02)00588-X, 2003.
- Coale, K. H., Michael Gordon, R., and Wang, X.: The distribution and behavior of dissolved and particulate iron and zinc in the Ross Sea and Antarctic circumpolar current along 170° W, Deep Sea Res. Part Oceanogr. Res. Pap., 52, 295–318, https://doi.org/10.1016/j.dsr.2004.09.008, 2005.
- Cohen, N. R., McIlvin, M. R., Moran, D. M., Held, N. A., Saunders, J. K., Hawco, N. J., Brosnahan, M., DiTullio, G. R., Lamborg, C., McCrow, J. P., Dupont, C. L., Allen, A. E., and Saito, M. A.: Dinoflagellates alter their carbon and nutrient metabolic strategies across environmental gradients in the central Pacific Ocean,

- Nat. Microbiol., 6, 173–186, https://doi.org/10.1038/s41564-020-00814-7, 2021.
- Cox, A. D., Noble, A. E., and Saito, M. A.: Cadmium enriched stable isotope uptake and addition experiments with natural phytoplankton assemblages in the Costa Rica Upwelling Dome, Mar. Chem., 166, 70–81, https://doi.org/10.1016/j.marchem.2014.09.009, 2014.
- Crameri, F.: Scientific colour maps (8.0.1), Zenodo [data set], https://doi.org/10.5281/zenodo.8409685, 2023.
- Crawford, D. W., Lipsen, M. S., Purdie, D. A., Lohan, M. C., Statham, P. J., Whitney, F. A., Putland, J. N., Johnson, W. K., Sutherland, N., Peterson, T. D., Harrison, P. J., and Wong, C. S.: Influence of zinc and iron enrichments on phytoplankton growth in the northeastern subarctic Pacific, Limnol. Oceanogr., 48, 1583–1600, https://doi.org/10.4319/lo.2003.48.4.1583, 2003.
- Cullen, J. T., Lane, T. W., Morel, F. M. M., and Sherrell, R. M.: Modulation of cadmium uptake in phytoplankton by seawater CO<sub>2</sub> concentration, Nature, 402, 165–167, https://doi.org/10.1038/46007, 1999.
- Cutter, G. A. and Bruland, K. W.: Rapid and noncontaminating sampling system for trace elements in global ocean surveys, Limnol. Oceanogr.-Methods, 10, 425–436, https://doi.org/10.4319/lom.2012.10.425, 2012.
- Dai, M., Su, J., Zhao, Y., Hofmann, E. E., Cao, Z., Cai, W.-J., Gan, J., Lacroix, F., Laruelle, G. G., Meng, F., Müller, J. D., Regnier, P. A. G., Wang, G., and Wang, Z.: Carbon Fluxes in the Coastal Ocean: Synthesis, Boundary Processes, and Future Trends, Annu. Rev. Earth Planet. Sci., 50, 593–626, https://doi.org/10.1146/annurev-earth-032320-090746, 2022.
- DeJong, H. B., Dunbar, R. B., Mucciarone, D., and Koweek, D. A.: Carbonate saturation state of surface waters in the Ross Sea and Southern Ocean: controls and implications for the onset of aragonite undersaturation, Biogeosciences, 12, 6881–6896, https://doi.org/10.5194/bg-12-6881-2015, 2015.
- Dickson, A. G., Sabine, C. L., and Christian, J. R.: Guide to best practices for ocean CO<sub>2</sub> measurement, North Pacific Marine Science Organization, https://doi.org/10.25607/OBP-1342, 2007.
- DiTullio, G.: pCO2 (LDEO pCO2) data as collected during the cruise NBP1801, Ditullio/B-007; Dunbar/O-131; Saba/B-050, Rolling Deck to Repository (R2R) [data set], https://doi.org/10.7284/139318, 2017.
- DiTullio, G.: Nathaniel B. Palmer CRUISE ID NBP1801, Rolling Deck to Repository (R2R) [data set], https://doi.org/10.7284/907753, 2018.
- DiTullio, G. and Lee, P.: Hydrographic data collected by CTD during RVIB Nathaniel B. Palmer cruise in the Ross Sea, Southern Ocean from 2017-2018, Biological and Chemical Oceanography Data Management Office [data set], https://doi.org/10.1575/1912/bco-dmo.783911.1, 2020.
- DiTullio, G. R. and Smith, W. O.: Spatial patterns in phytoplankton biomass and pigment distributions in the Ross Sea, J. Geophys. Res.-Oceans, 101, 18467–18477, https://doi.org/10.1029/96JC00034, 1996.
- DiTullio, G. R., Grebmeier, J. M., Arrigo, K. R., Lizotte, M. P., Robinson, D. H., Leventer, A., Barry, J. P., VanWoert, M. L., and Dunbar, R. B.: Rapid and early export of Phaeocystis antarctica blooms in the Ross Sea, Antarctica, Nature, 404, 595–598, https://doi.org/10.1038/35007061, 2000.

- DiTullio, G. R., Geesey, M. E., Leventer, A., and Lizotte, M. P.: Algal pigment ratios in the Ross Sea: Implications for Chemtax analysis of Southern Ocean data, in: Biogeochemistry of the Ross Sea, 78, 35–51, https://doi.org/10.1029/078ARS03, 2003.
- DiTullio, G. R., Garcia, N., Riseman, S. F., and Sedwick, P. N.: Effects of iron concentration on pigment composition in Phaeocystis antarctica grown at low irradiance, Biogeochemistry, 83, 71–81, https://doi.org/10.1007/s10533-007-9080-8, 2007.
- Dreux Chappell, P., Vedmati, J., Selph, K. E., Cyr, H. A., Jenkins, B. D., Landry, M. R., and Moffett, J. W.: Preferential depletion of zinc within Costa Rica upwelling dome creates conditions for zinc co-limitation of primary production, J. Plankton Res., 38, 244–255, https://doi.org/10.1093/plankt/fbw018, 2016.
- Eddy, S. R.: Accelerated Profile HMM Searches, PLoS Comput. Biol., 7, e1002195, https://doi.org/10.1371/journal.pcbi.1002195, 2011.
- Edmonds, K. A., Jordan, M. R., and Giedroc, D. P.: COG0523 proteins: a functionally diverse family of transition metal-regulated G3E P-loop GTP hydrolases from bacteria to man, Metallomics, 13, mfab046, https://doi.org/10.1093/mtomcs/mfab046, 2021.
- Ellwood, M. J.: Zinc and cadmium speciation in subantarctic waters east of New Zealand, Mar. Chem., 87, 37–58, https://doi.org/10.1016/j.marchem.2004.01.005, 2004.
- Emms, D. M. and Kelly, S.: SHOOT: phylogenetic gene search and ortholog inference, Genome Biol., 23, 85, https://doi.org/10.1186/s13059-022-02652-8, 2022.
- Etheridge, D. M., Steele, L. P., Langenfelds, R. L., Francey, R. J., Barnola, J.-M., and Morgan, V. I.: Natural and anthropogenic changes in atmospheric CO<sub>2</sub> over the last 1000 years from air in Antarctic ice and firn, J. Geophys. Res.-Atmos., 101, 4115–4128, https://doi.org/10.1029/95JD03410, 1996.
- Fitzwater, S. E., Johnson, K. S., Gordon, R. M., Coale, K. H., and Smith, W. O.: Trace metal concentrations in the Ross Sea and their relationship with nutrients and phytoplankton growth, Deep-Sea Res. Part II Top. Stud. Oceanogr., 47, 3159–3179, https://doi.org/10.1016/S0967-0645(00)00063-1, 2000.
- Fourquez, M., Bressac, M., Deppeler, S. L., Ellwood, M., Obernosterer, I., Trull, T. W., and Boyd, P. W.: Microbial Competition in the Subpolar Southern Ocean: An Fe–C Co-limitation Experiment, Front. Mar. Sci., 6, 776, https://doi.org/10.3389/fmars.2019.00776, 2020.
- Franck, V., Bruland, K., Hutchins, D., and Brzezinski, M.: Iron and zinc effects on silicic acid and nitrate uptake kinetics in three high-nutrient, low-chlorophyll (HNLC) regions, Mar. Ecol. Prog. Ser., 252, 15–33, https://doi.org/10.3354/meps252015, 2003.
- Harrison, C. S., Long, M. C., Lovenduski, N. S., and Moore, J. K.: Mesoscale Effects on Carbon Export: A Global Perspective, Global Biogeochem. Cy., 32, 680–703, https://doi.org/10.1002/2017GB005751, 2018.
- Jakuba, R. W., Saito, M. A., Moffett, J. W., and Xu, Y.: Dissolved zinc in the subarctic North Pacific and Bering Sea: Its distribution, speciation, and importance to primary producers, Global Biogeochem. Cy., 26, GB2015, https://doi.org/10.1029/2010GB004004, 2012.
- Jensen, E. L., Maberly, S. C., and Gontero, B.: Insights on the Functions and Ecophysiological Relevance of the Diverse Carbonic Anhydrases in Microalgae, Int. J. Mol. Sci., 21, 2922, https://doi.org/10.3390/ijms21082922, 2020a.

- Jensen, L. T., Wyatt, N. J., Landing, W. M., and Fitzsimmons, J. N.: Assessment of the stability, sorption, and exchangeability of marine dissolved and colloidal metals, Mar. Chem., 220, 103754, https://doi.org/10.1016/j.marchem.2020.103754, 2020b.
- Jiang, L., Dunne, J., Carter, B. R., Tjiputra, J. F., Terhaar, J., Sharp, J. D., Olsen, A., Alin, S., Bakker, D. C. E., Feely, R. A., Gattuso, J., Hogan, P., Ilyina, T., Lange, N., Lauvset, S. K., Lewis, E. R., Lovato, T., Palmieri, J., Santana-Falcón, Y., Schwinger, J., Séférian, R., Strand, G., Swart, N., Tanhua, T., Tsujino, H., Wanninkhof, R., Watanabe, M., Yamamoto, A., and Ziehn, T.: Global Surface Ocean Acidification Indicators From 1750 to 2100, J. Adv. Model. Earth Syst., 15, e2022MS003563, https://doi.org/10.1029/2022MS003563, 2023.
- Keeling, C. D., Bacastow, R. B., Bainbridge, A. E., Ekdahl, C. A., Guenther, P. R., Waterman, L. S., and Chin, J. F. S.: Atmospheric carbon dioxide variations at Mauna Loa Observatory, Hawaii, Tellus Dyn. Meteorol. Oceanogr., 28, 538, https://doi.org/10.3402/tellusa.v28i6.11322, 1976.
- Kell, R. M., Chmiel, R. J., Rao, D., Moran, D. M., McIlvin, M. R., Horner, T. J., Schanke, N. L., Sugiyama, I., Dunbar, R. B., DiTullio, G. R., and Saito, M. A.: High metabolic zinc demand within native Amundsen and Ross sea phytoplankton communities determined by stable isotope uptake rate measurements, Biogeosciences, 21, 5685–5706, https://doi.org/10.5194/bg-21-5685-2024, 2024.
- Kellogg, R. M., McIlvin, M. R., Vedamati, J., Twining, B. S., Moffett, J. W., Marchetti, A., Moran, D. M., and Saito, M. A.: Efficient zinc/cobalt inter-replacement in northeast Pacific diatoms and relationship to high surface dissolved Co: Zn ratios, Limnol. Oceanogr., 65, 2557–2582, https://doi.org/10.1002/lno.11471, 2020.
- Kellogg, R. M., Moosburner, M. A., Cohen, N. R., Hawco, N. J., McIlvin, M. R., Moran, D. M., DiTullio, G. R., Subhas, A. V., Allen, A. E., and Saito, M. A.: Adaptive responses of marine diatoms to zinc scarcity and ecological implications, Nature Communications, 13, 1–13, https://doi.org/10.1038/s41467-022-29603-y, 2022a.
- Kellogg, R. M., Moran, D. M., McIlvin, M. R., Subhas, A. V., Allen, A. E., and Saito, M. A.: Lack of a Zn/Co substitution ability in the polar diatom *Chaetoceros neogracile* RS19, Limnol. Oceanogr., 67, 2265–2280, https://doi.org/10.1002/lno.12201, 2022b.
- Krogh, A., Larsson, B., von Heijne, G., and Sonnhammer, E. L. L.: Predicting transmembrane protein topology with a hidden markov model: application to complete genomes, J. Mol. Biol., 305, 567–580, https://doi.org/10.1006/jmbi.2000.4315, 2001.
- Krumhardt, K. M., Lovenduski, N. S., Iglesias-Rodriguez, M. D., and Kleypas, J. A.: Coccolithophore growth and calcification in a changing ocean, Prog. Oceanogr., 159, 276–295, https://doi.org/10.1016/j.pocean.2017.10.007, 2017.
- Lampe, R. and Allen, A.: Metatranscriptome assembly and annotations for CICLOPS (NBP1801), Zenodo [data set], https://doi.org/10.5281/zenodo.17307449, 2025.
- Lampe, R., Kell, R. M., and Saito, M.: CICLOPS Project (Cruise NBP1801) Data Overview, Zenodo [data set], https://doi.org/10.5281/zenodo.17287908, 2025.
- Lampe, R. H., Mann, E. L., Cohen, N. R., Till, C. P., Thamatrakoln,K., Brzezinski, M. A., Bruland, K. W., Twining, B. S., andMarchetti, A.: Different iron storage strategies among bloom-

- forming diatoms, P. Natl. Acad. Sci. USA, 115, E12275–E12284, https://doi.org/10.1073/pnas.1805243115, 2018.
- Lane, T. W. and Morel, F. M.: A biological function for cadmium in marine diatoms, P. Natl. Acad. Sci. USA, 97, 4627–31, https://doi.org/10.1073/pnas.090091397, 2000a.
- Lane, T. W. and Morel, F. M. M.: Regulation of Carbonic Anhydrase Expression by Zinc, Cobalt, and Carbon Dioxide in the Marine Diatom Thalassiosira weissflogii, Plant Physiol., 123, 345–352, https://doi.org/10.1104/pp.123.1.345, 2000b.
- Lauvset, S. K., Lange, N., Tanhua, T., Bittig, H. C., Olsen, A., Kozyr, A., Alin, S., Álvarez, M., Azetsu-Scott, K., Barbero, L., Becker, S., Brown, P. J., Carter, B. R., da Cunha, L. C., Feely, R. A., Hoppema, M., Humphreys, M. P., Ishii, M., Jeansson, E., Jiang, L.-Q., Jones, S. D., Lo Monaco, C., Murata, A., Müller, J. D., Pérez, F. F., Pfeil, B., Schirnick, C., Steinfeldt, R., Suzuki, T., Tilbrook, B., Ulfsbo, A., Velo, A., Woosley, R. J., and Key, R. M.: GLODAPv2.2022: the latest version of the global interior ocean biogeochemical data product, Earth Syst. Sci. Data, 14, 5543–5572, https://doi.org/10.5194/essd-14-5543-2022, 2022.
- Lhospice, S., Gomez, N. O., Ouerdane, L., Brutesco, C., Ghssein, G., Hajjar, C., Liratni, A., Wang, S., Richaud, P., Bleves, S., Ball, G., Borezée-Durant, E., Lobinski, R., Pignol, D., Arnoux, P., and Voulhoux, R.: Pseudomonas aeruginosa zinc uptake in chelating environment is primarily mediated by the metallophore pseudopaline, Sci. Rep.-UK, 7, 17132, https://doi.org/10.1038/s41598-017-16765-9, 2017.
- Li, B. and Dewey, C. N.: RSEM: accurate transcript quantification from RNA-Seq data with or without a reference genome, BMC Bioinformatics, 12, 323, https://doi.org/10.1186/1471-2105-12-323, 2011.
- Lohan, M. C., Statham, P. J., and Crawford, D. W.: Total dissolved zinc in the upper water column of the subarctic North East Pacific, Deep-Sea Res. Part II Top. Stud. Oceanogr., 49, 5793– 5808, https://doi.org/10.1016/S0967-0645(02)00215-1, 2002.
- Lu, X. and Zhu, H.: Tube-Gel Digestion, Mol. Cell. Proteomics, 4, 1948–1958, https://doi.org/10.1074/mcp.m500138-mcp200, 2005.
- Mangoni, O., Saggiomo, M., Bolinesi, F., Castellano, M., Povero, P., Saggiomo, V., and DiTullio, G. R.: Phaeocystis antarctica unusual summer bloom in stratified antarctic coastal waters (Terra Nova Bay, Ross Sea), Mar. Environ. Res., 151, 104733, https://doi.org/10.1016/j.marenvres.2019.05.012, 2019.
- Martin, J. H., Fitzwater, S. E., and Gordon, R. M.: Iron deficiency limits phytoplankton growth in Antarctic waters, Global Biogeochem. Cy., 4, 5–12, https://doi.org/10.1029/GB004i001p00005, 1990.
- Mazzotta, M. G., McIlvin, M. R., Moran, D. M., Wang, D. T., Bidle, K. D., Lamborg, C. H., and Saito, M. A.: Characterization of the metalloproteome of Pseudoalteromonas (BB2-AT2): biogeochemical underpinnings for zinc, manganese, cobalt, and nickel cycling in a ubiquitous marine heterotroph, Metallomics, 13, mfab060, https://doi.org/10.1093/mtomcs/mfab060, 2021.
- McIlvin, M. R. and Saito, M. A.: Online Nanoflow Two-Dimension Comprehensive Active Modulation Reversed Phase–Reversed Phase Liquid Chromatography High-Resolution Mass Spectrometry for Metaproteomics of Environmental and Microbiome Samples, J. Proteome Res., 20, 4589–4597, https://doi.org/10.1021/acs.jproteome.1c00588, 2021.

- Middag, R., De Baar, H. J. W., and Bruland, K. W.: The Relationships Between Dissolved Zinc and Major Nutrients Phosphate and Silicate Along the GEOTRACES GA02 Transect in the West Atlantic Ocean, Global Biogeochem. Cy., 33, 63–84, https://doi.org/10.1029/2018GB006034, 2019.
- Milner, M. J., Seamon, J., Craft, E., and Kochian, L. V.: Transport properties of members of the ZIP family in plants and their role in Zn and Mn homeostasis, J. Exp. Bot., 64, 369–381, https://doi.org/10.1093/jxb/ers315, 2013.
- Moore, C. M., Mills, M. M., Arrigo, K. R., Berman-Frank, I., Bopp, L., Boyd, P. W., Galbraith, E. D., Geider, R. J., Guieu, C., Jaccard, S. L., Jickells, T. D., La Roche, J., Lenton, T. M., Mahowald, N. M., Marañón, E., Marinov, I., Moore, J. K., Nakatsuka, T., Oschlies, A., Saito, M. A., Thingstad, T. F., Tsuda, A., and Ulloa, O.: Processes and patterns of oceanic nutrient limitation, Nat. Geosci., 6, 701–710, https://doi.org/10.1038/ngeo1765, 2013.
- Morel, F. M. M., Reinfelder, J. R., Roberts, S. B., Chamberlain, C. P., Lee, J. G., and Yee, D.: Zinc and carbon colimitation of marine phytoplankton, Nature, 369, 740–742, https://doi.org/10.1038/369740A0, 1994.
- Mortazavi, A., Williams, B. A., McCue, K., Schaeffer, L., and Wold, B.: Mapping and quantifying mammalian transcriptomes by RNA-Seq, Nat. Methods, 5, 621–628, https://doi.org/10.1038/nmeth.1226, 2008.
- Obernosterer, I., Fourquez, M., and Blain, S.: Fe and C colimitation of heterotrophic bacteria in the naturally fertilized region off the Kerguelen Islands, Biogeosciences, 12, 1983–1992, https://doi.org/10.5194/bg-12-1983-2015, 2015.
- Podell, S. and Gaasterland, T.: DarkHorse: a method for genome-wide prediction of horizontal gene transfer, Genome Biol., 8, R16, https://doi.org/10.1186/gb-2007-8-2-r16, 2007.
- Rapp, I., Schlosser, C., Rusiecka, D., Gledhill, M., and Achterberg, E. P.: Automated preconcentration of Fe, Zn, Cu, Ni, Cd, Pb, Co, and Mn in seawater with analysis using high-resolution sector field inductively-coupled plasma mass spectrometry, Anal. Chim. Acta, 976, 1–13, https://doi.org/10.1016/j.aca.2017.05.008, 2017.
- Redfield, A. C.: The Biological Control of Chemical Factors in the Environment, Am. Sci., 46, 230A, 205–221, https://www.jstor.org/stable/27827150 (last access: 17 October 2025), 1958.
- Rho, M., Tang, H., and Ye, Y.: FragGeneScan: predicting genes in short and error-prone reads, Nucleic Acids Res., 38, e191–e191, https://doi.org/10.1093/nar/gkq747, 2010.
- Riebesell, U., Wolf-Gladrow, D. A., and Smetacek, V.: Carbon dioxide limitation of marine phytoplankton growth rates, Nature, 361, 249–251, https://doi.org/10.1038/361249a0, 1993.
- Robbins, L. L., Daly, K. L., Barbero, L., Wanninkhof, R., He, R., Zong, H., Lisle, J. T., Cai, W. -J., and Smith, C. G.: Spatial and Temporal Variability of *p*CO<sub>2</sub>, Carbon Fluxes, and Saturation State on the West Florida Shelf, J. Geophys. Res.-Oceans, 123, 6174–6188, https://doi.org/10.1029/2018JC014195, 2018.
- Roshan, S., DeVries, T., Wu, J., and Chen, G.: The Internal Cycling of Zinc in the Ocean, Global Biogeochem. Cy., 32, 1833–1849, https://doi.org/10.1029/2018GB006045, 2018.
- Saito, M. A. and Goepfert, T. J.: Zinc-cobalt colimitation of *Phaeocystis antarctica*, Limnol. Oceanogr., 53, 266–275, https://doi.org/10.4319/lo.2008.53.1.0266, 2008.

- Saito, M. A., Goepfert, T. J., and Ritt, J. T.: Some thoughts on the concept of colimitation: Three definitions and the importance of bioavailability, Limnol. Oceanogr., 53, 276–290, https://doi.org/10.4319/lo.2008.53.1.0276, 2008.
- Schanke, N. L., Bolinesi, F., Mangoni, O., Katlein, C., Anhaus, P., Hoppmann, M., Lee, P. A., and DiTullio, G. R.: Biogeochemical and ecological variability during the late summerearly autumn transition at an ice-floe drift station in the Central Arctic Ocean, Limnol. Oceanogr., 66, S363–S382, https://doi.org/10.1002/lno.11676, 2021.
- Scharek, R., Van Leeuwe, M. A., and De Baar, H. J. W.: Responses of Southern Ocean phytoplankton to the addition of trace metals, Deep-Sea Res. Part II Top. Stud. Oceanogr., 44, 209–227, https://doi.org/10.1016/S0967-0645(96)00074-4, 1997.
- Schlitzer, R.: Ocean Data View, https://odv.awi.de (last access: 29 September 2025), 2025.
- Schmieder, R., Lim, Y. W., and Edwards, R.: Identification and removal of ribosomal RNA sequences from metatranscriptomes, Bioinformatics, 28, 433–435, https://doi.org/10.1093/bioinformatics/btr669, 2012.
- Schneider, B. and Müller, J. D.: Biogeochemical Transformations in the Baltic Sea: Observations Through Carbon Dioxide Glasses, Springer International Publishing AG, Cham, ISBN 978-3-319-61699-5, https://doi.org/10.1007/978-3-319-61699-5, 110 pp., 2018.
- Sedwick, P. N., Marsay, C. M., Sohst, B. M., Aguilar-Islas, A. M., Lohan, M. C., Long, M. C., Arrigo, K. R., Dunbar, R. B., Saito, M. A., Smith, W. O., and DiTullio, G. R.: Early season depletion of dissolved iron in the Ross Sea polynya: Implications for iron dynamics on the Antarctic continental shelf, J. Geophys. Res., 116, C12019, https://doi.org/10.1029/2010JC006553, 2011.
- Sharp, J. D., Pierrot, D., Humphreys, M. P., Epitalon, J.-M., Orr, J. C., Lewis, E. R., and Wallace, D. W. R.: CO2SYSv3 for MATLAB, Zenodo [code], https://doi.org/10.5281/ZENODO.3950562, 2023.
- Shim, J., Kim, D., Kang, Y. C., Lee, J. H., Jang, S.-T., and Kim, C.-H.: Seasonal variations in pCO<sub>2</sub> and its controlling factors in surface seawater of the northern East China Sea, Cont. Shelf Res., 27, 2623–2636, https://doi.org/10.1016/j.csr.2007.07.005, 2007.
- Sieber, M., Conway, T. M., de Souza, G. F., Hassler, C. S., Ellwood, M. J., and Vance, D.: Cycling of zinc and its isotopes across multiple zones of the Southern Ocean: Insights from the Antarctic Circumnavigation Expedition, Geochim. Cosmochim. Acta, 268, 310–324, https://doi.org/10.1016/j.gca.2019.09.039, 2020.
- Smith, W. O., Shields, A. R., Peloquin, J. A., Catalano, G., Tozzi, S., Dinniman, M. S., and Asper, V. A.: Interannual variations in nutrients, net community production, and biogeochemical cycles in the Ross Sea, Deep-Sea Res. Part II Top. Stud. Oceanogr., 53, 815–833, https://doi.org/10.1016/j.dsr2.2006.02.014, 2006.
- Sperfeld, E., Raubenheimer, D., and Wacker, A.: Bridging factorial and gradient concepts of resource co-limitation: towards a general framework applied to consumers, Ecol. Lett., 19, 201–215, https://doi.org/10.1111/ele.12554, 2016.
- Subhas, A. V., Adkins, J. F., Dong, S., Rollins, N. E., and Berelson, W. M.: The carbonic anhydrase activity of sinking and suspended particles in the North Pacific Ocean, Limnol. Oceanogr., 65, 637– 651, https://doi.org/10.1002/lno.11332, 2019.

- Sun, Y., Debeljak, P., and Obernosterer, I.: Microbial iron and carbon metabolism as revealed by taxonomy-specific functional diversity in the Southern Ocean, ISME J., 15, 2933–2946, https://doi.org/10.1038/s41396-021-00973-3, 2021.
- Sunda, W. G. and Huntsman, S. A.: Cobalt and zinc interreplacement in marine phytoplankton: Biological and geochemical implications, Limnol. Oceanogr., 40, 1404–1417, https://doi.org/10.4319/lo.1995.40.8.1404, 1995.
- Sunda, W. G. and Huntsman, S. A.: Effect of Zn, Mn, and Fe on Cd accumulation in phytoplankton: Implications for oceanic Cd cycling, Limnol. Oceanogr., 45, 1501–1516, https://doi.org/10.4319/lo.2000.45.7.1501, 2000.
- Sunda, W. G. and Huntsman, S. A.: Effect of CO<sub>2</sub> supply and demand on zinc uptake and growth limitation in a coastal diatom, Limnol. Oceanogr., 50, 1181–1192, https://doi.org/10.4319/lo.2005.50.4.1181, 2005.
- Takahashi, T., Sutherland, S. C., and Kozyr, A.: Global Ocean Surface Water Partial Pressure of CO<sub>2</sub> Database (LDEO Database Version 2019): Measurements Performed During 1957–2019 (NCEI Accession 0160492), NOAA Natl. Cent. Environ. Inf., 2020.
- Tatusov, R. L., Fedorova, N. D., Jackson, J. D., Jacobs, A. R., Kiryutin, B., Koonin, E. V., Krylov, D. M., Mazumder, R., Mekhedov, S. L., Nikolskaya, A. N., Rao, B. S., Smirnov, S., Sverdlov, A. V., Vasudevan, S., Wolf, Y. I., Yin, J. J., and Natale, D. A.: The COG database: an updated version includes eukaryotes, BMC Bioinformatics, 4, 41, https://doi.org/10.1186/1471-2105-4-41, 2003.
- Tortell, P. D., Payne, C., Gueguen, C., Strzepek, R. F., Boyd, P. W., and Rost, B.: Inorganic carbon uptake by Southern Ocean phytoplankton, Limnol. Oceanogr., 53, 1266–1278, https://doi.org/10.4319/lo.2008.53.4.1266, 2008.
- Tortell, P. D., Long, M. C., Payne, C. D., Alderkamp, A.-C., Dutrieux, P., and Arrigo, K. R.: Spatial distribution of *p*CO<sub>2</sub>, ΔO<sub>2</sub>/Ar and dimethylsulfide (DMS) in polynya waters and the sea ice zone of the Amundsen Sea, Antarctica, Deep-Sea Res. Part II, 71–76, 77–93, https://doi.org/10.1016/j.dsr2.2012.03.010, 2012.
- Twining, B. S. and Baines, S. B.: The trace metal composition of marine phytoplankton, Annu. Rev. Mar. Sci., 5, 191–215, https://doi.org/10.1146/annurev-marine-121211-172322, 2013.
- Valerio, A. M., Kampel, M., Ward, N. D., Sawakuchi, H. O., Cunha, A. C., and Richey, J. E.: CO<sub>2</sub> partial pressure and fluxes in the Amazon River plume using in situ and remote sensing data, Cont. Shelf Res., 215, 104348, https://doi.org/10.1016/j.csr.2021.104348, 2021.
- Wuttig, K., Townsend, A. T., van der Merwe, P., Gault-Ringold, M., Holmes, T., Schallenberg, C., Latour, P., Tonnard, M., Rijkenberg, M. J. A., Lannuzel, D., and Bowie, A. R.: Critical evaluation of a seaFAST system for the analysis of trace metals in marine samples, Talanta, 197, 653–668, https://doi.org/10.1016/j.talanta.2019.01.047, 2019.
- Wyatt, N. J., Milne, A., Woodward, E. M. S., Rees, A. P., Browning, T. J., Bouman, H. A., Worsfold, P. J., and Lohan, M. C.: Biogeochemical cycling of dissolved zinc along the GEOTRACES South Atlantic transect GA10 at 40° S, Global Biogeochem. Cy., 28, 44–56, https://doi.org/10.1002/2013GB004637, 2014.
- Xu, Y., Shi, D., Aristilde, L., and Morel, F. M. M.: The effect of pH on the uptake of zinc and cadmium in marine phytoplankton:

Possible role of weak complexes, Limnol. Oceanogr., 57, 293–304, https://doi.org/10.4319/lo.2012.57.1.0293, 2012.

Ye, N., Han, W., Toseland, A., Wang, Y., Fan, X., Xu, D., Van Oosterhout, C., Sea of Change Consortium, Aslam, S. N., Barry, K., Beszteri, B., Brussaard, C., Clum, A., Copeland, A., Daum, C., Duncan, A., Eloe-Fadrosh, E., Fong, A., Foster, B., Foster, B., Ginzburg, M., Huntemann, M., Ivanova, N. N., Kyrpides, N. C., Martin, K., Moulton, V., Mukherjee, S., Palaniappan, K., Reddy, T. B. K., Roux, S., Schmidt, K., Strauss, J., Timmermans, K., Tringe, S. G., Underwood, G. J. C., Valentin, K. U., Van De Poll, W. H., Varghese, N., Grigoriev, I. V., Tagliabue, A., Zhang, J., Zhang, Y., Ma, J., Qiu, H., Li, Y., Zhang, X., and Mock, T.: The role of zinc in the adaptive evolution of polar phytoplankton, Nat. Ecol. Evol., 6, 965–978, https://doi.org/10.1038/s41559-022-01750-x, 2022.

Zhang, Y., Wen, Z., Washburn, M. P., and Florens, L.: Refinements to Label Free Proteome Quantitation: How to Deal with Peptides Shared by Multiple Proteins, Anal. Chem., 82, 2272–2281, https://doi.org/10.1021/ac9023999, 2010.